THE JOURNAL OF PHYSICAL CHEMISTRY C

pubs.acs.org/JPCC Article

# Effects of van der Waals Dispersion Interactions in Density Functional Studies of Adsorption, Catalysis, and Tribology on Metals

Dingwang Yuan,△ Yanning Zhang,△ Wilson Ho, and Ruqian Wu*

Cite This: J. Phys. Chem. C 2020, 124, 16926−16942 Read Online

ACCESS | Metrics & More | Article Recommendations

**ABSTRACT:** We review the effect of van der Waals (vdW) dispersion interactions on the determination of adsorption energy, vibration frequency, catalytic activity, and tribological property of weak physisorption systems through modern density functional theory calculations for prototypical systems. The inclusion of vdW corrections is crucial in many cases for studies of catalytic reaction rates and even pathways as well as for the understanding of puzzling observations for tribological properties of rare gas layers on noble metals. We comment on the noticeable discrepancies as different vdW functionals are adopted and suggest more stringent tests against new experimental results such as frequencies of low-energy external vibrations modes for the further development of more universal vdW functionals.

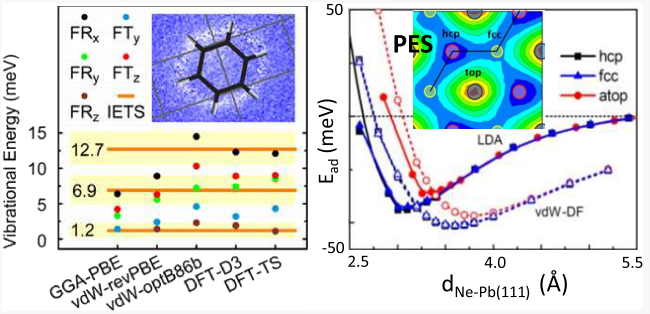


## 1. INTRODUCTION

The nature of complex interactions between adsorbates and substrates is an important topic in major chemistry and physics textbooks for years. Recently, the understanding of weak van der Waals (vdW), hydrogen and halogen bonds in molecular systems attracts increasing attention as they play a vital role in many fundamental research areas from biomaterials, heterogeneous catalysis, and electrocatalysis[1−6] to the tribological properties.[7] The continuous advances of experimental techniques[8−10] and computational modeling packages[11] make it possible to quantitatively describe the weak interactions between atoms, molecules, and thin films on diverse substrates, and weak bonds can be directly imaged, manipulated, and calculated. In the experimental side, these interactions, e.g., between adsorbates and metal substrates, can be quantitatively characterized with high chemical accuracy using single crystal adsorption calorimetry (SCAC),[12] single-molecule inelastic tunneling probe (itProbe) based on scanning tunneling microscopy (STM),[8−10] high-spatial-resolution atomic force microscopy (AFM),[13] and normal-incidence X-ray standing wave (NIXSW) methods.[14] Combining temperature-programmed desorption (TPD) and SCAC techniques, Campbell *et al.* reported accurate measurements of adsorption energies including the strengths of vdW interactions for a variety of systems.[15−20] The chemical reaction kinetics of molecules can be quantitatively characterized by many other techniques such as X-ray photoelectron spectroscopy (XPS; by following the spectroscopic features of reactants) and time-resolved infrared reflection absorption spectroscopy (TR-IRAS).[21] Notably, the newly developed itProbe technique based on STM with a CO-functionalized tip may directly map the weak vdW and halogen bonds in many systems such as Xe/Ag(110),[9] benzene/Ag(110),[22] and fluorobenzene or bromobenzene molecules adsorbed on Ag(110)[8] with a sub-Angstrom spatial resolution. These developments provide comprehensive databases for benchmarking the development of reliable and transferrable vdW functionals that may improve the first-principles studies of physisorption and catalytic reaction of diverse systems toward the chemical accuracy.

Another important area of studying weak bonds is tribology. The mechanism of energy dissipation in inert molecular or atomic layers moving on substrates is crucial for understanding and manipulating tribological properties of lubricated interfaces. Quantitative measurements of resistive barriers can be achieved with apparatuses such as a quartz crystal microbalance, friction force microscope, and high-resolution helium atom scattering (HAS) at microscopic and macroscopic length scales.[23−25] Particularly, systems with adsorption of rare-gas (RG) atoms on solid surfaces are prototypes for exploring the influences of vdW interactions on the tribological properties at the atomic level.[26−32] As an example of the puzzles in this realm, Bruschi *et al.* found a drastic difference between the

Received: March 15, 2020
Revised: June 26, 2020
Published: July 10, 2020







https://dx.doi.org/10.1021/acs.jpcc.0c02293
J. Phys. Chem. C 2020, 124, 16926−16942

sliding friction of Ne and Kr mono- or multilayers: while Ne layers may slide on Pb(111) with a measurable slip time (~3 ns), the slipping rate of Kr layers is essentially zero at a low temperature (~6.5 K).[26,27] This appeared as a surprise because of the similarity between these RG atoms in many occasions and could only be understood through density functional theory (DFT) simulations with the inclusion of vdW interactions.[24] Reliable determination of energy barriers at the millielectronvolt level for the sliding and rotating motions between two inert substances becomes ever important nowadays as heterostructures of different vdW two-dimensional (2D) materials are probably the richest mine for the generation of emergent quantum properties.

It is recognized that the DFT within the frameworks of local density approximation (LDA) or generalized gradient approximation (GGA) is unreliable for the description of systems with weak interactions.[11,12,24] Particularly, for systems with non-covalent bonding, the dynamical correlations between fluctuating charge distributions, i.e., vdW dispersion interactions, have important effects on adsorption energies, reaction/diffusion barriers, and even geometric configurations. In the past decade, many schemes were developed to improve the description for the van der Waals dispersion interactions in the DFT framework[33] and the field has greatly advanced toward the chemical accuracy to make realistic predictions as required for many challenging issues in chemistry, physics, materials science, and nanoscience.

The purpose of this review is to give an overview of using different vdW schemes for theoretical studies of various weak bond systems, primarily with examples of our own studies of adsorptions, chemical reactions, and tribological properties. Most of these studies were done through close collaborations with experimental groups, and hence the side-by-side comparisons to dependable experimental data allowed stringent examinations for the performance of different vdW functionals. We first give a summary for different vdW schemes and discuss their performance for the determination of adsorption energies of typical weak bond systems. More stringent tests are given through calculations of low-energy molecular vibrational modes and comparisons with corresponding experimental results. Furthermore, we show examples of several recent studies of catalytic activity and selectivity using different vdW functionals. Finally, we discuss applications of vdW-inclusive DFT methods for the determination of tribological properties of several inert layers on solid surfaces.

## 2. VAN DER WAALS-INCLUSIVE DENSITY FUNCTIONAL THEORY METHODS

It is recognized that the vdW interaction results from three sources: (1) the electrostatic force between two permanent dipoles, (2) the inductive force between a permanent dipole and an induced dipole, and (3) the dispersion force between two spontaneously induced dipoles. The first two dipole−dipole interactions can be well treated by semilocal density functionals. The last one, also called the London dispersion force, associates with the correlated fluctuations between electrons in two sides and cannot be described by conventional density functionals. At the present, numerous vdW correction schemes are available by adding, e.g., pairwise interatomic attraction terms, the random phase expression of correlation energy, or the non-local correlation energy in DFT calculations. These developments have been implemented in different DFT codes, including Q-Chem, SIESTA, VASP, CASTEP, Quantum espresso, FHi-aims, etc.[33] Systematic tests have been performed for the performance of different vdW-DFT methods for the determination of physical properties of solids and molecules, such as adsorption energies, surface energies, stacking fault energies, and reaction energy barriers.[11,34−39] While significant improvements were found over the conventional GGA functionals in almost all cases, different vdW methods still showed noticeable discrepancies. As the theoretical frameworks of the van der Waals-inclusive density functional theory have been rather extensively reviewed in the recent literature,[33,40−43] we only briefly summarize the main features of different vdW-inclusive DFT approaches in this section.

**2.1. DFT-D$_n$ Correction Methods.** To capture the long-range vdW dispersion interaction, the semi-empirical DFT-D$_n$-type ($n$ = 1−4) approaches add pairwise correction terms to the Kohn−Sham DFT energy ($E_{\text{KS-DFT}}$) in the form[40]

$$E_{\text{DFT}-\text{disp}} = E_{\text{KS}-\text{DFT}} + E_{\text{disp}} \tag{1}$$

The original vdW correction energy is computed by summing over all atomic pairs (denoted as A and B with a distance of $R_{\text{AB}}$) with element-dependent dispersion coefficients ($C_n$), damping functions ($f_{\text{damp},n}$), and scaling factors ($s_n$, $n$ = 6, 8, 10, ...):

$$E_{\text{disp}} = -\frac{1}{2}\sum_{\text{A}\neq\text{B}}\sum_{n=6,8,10} s_n \frac{C_n^{\text{AB}}}{R_{\text{AB}}^n} f_{\text{damp},n}(R_{\text{AB}}) \tag{2}$$

Depending on the way of constructing $C_n$ and $f_{\text{damp},n}$, several DFT-D versions are commonly used, such as DFT-D1/2/3,[44−47] DFT-TS,[48] DFT-TS+SCS,[49] DFT-TS+IH,[50,51] and DFT+dDsC.[52,53] In the DFT-D2 approach, for example, the dispersion coefficients are calculated from a formula that couples ionization potentials and static polarizabilities of isolated atoms. In the improved "DFT-D" schemes, the environmental dependence of $C_n$ coefficients is invoked by considering the number of neighbors. To avoid the overestimation of vdW interactions in small and medium ranges, the DFT-D3 scheme introduced a damping function $f_{\text{damp},n}$:[46,47]

$$f_{\text{damp},6}(R_{\text{AB}}) = \frac{1}{1 + 6(R_{\text{AB}}/(s_{r,6}R_0^{\text{AB}}))^{-\alpha_6}} \tag{3}$$

where $R_0^{\text{AB}}$ is the cutoff radius for atomic pair AB, $s_{r,6}$ is a functional-dependent scaling factor, and $\alpha_6$ is a parameter that determines the steepness of the function for a small $R_{\text{AB}}$. In this way, the dispersion coefficients are geometry-dependent (i.e., coordination number). In the newer DFT-D4 method,[54,55] the pairwise dipole−dipole dispersion coefficients are charge- and geometry-dependent. The DFT-dDsC and DFT-TS methods were proposed by Steinmann[52,53] and Tkatchenko and Scheffler,[48] with inclusion of charge-dependent dispersion and damping. In the DFT-TS/IH method,[50,51] the electron density of a molecule is subdivided with the Hirshfeld partitioning scheme, which may better describe properties of ionic solids. In the DFT-dDsC method, the dispersion coefficients are modeled by a generalized gradient-type approximation to Becke and Johnson's exchange hole dipole moment (XDM) formalism.[52,53,56]

Beyond schemes with atomic pairwise dispersion coefficients, the many-body dispersion (MBD) vdW functionals were developed recently. Based on the random phase approximation for the correlation energy, Tkatchenko *et al.*


https://dx.doi.org/10.1021/acs.jpcc.0c02293
J. Phys. Chem. C 2020, 124, 16926−16942

proposed the MBD@rsSCS method,[57,58] which was implemented in VASP by Bučko *et al.*[59] Additionally, in the DFT-D4 method the many-body dispersion energy can be calculated by adding higher-order dipole−dipole interactions based on the quantum harmonic oscillator (QHO) model.[54,55] The main advantage of DFT-$D_n$ methods is that they do not significantly increase the computing cost over the regular GGA level calculations.

**2.2. vdW-DF Methods.** More comprehensive van der Waals density functional (vdW-DF) approaches directly calculate the non-local correlation (dispersion) energy, in conjunction with an exchange part at the standard GGA level. The corrected exchange-correlation energy is written as $E_{xc} = E_x^{GGA} + E_c^{LDA} + E_c^{nl}$, where $E_x^{GGA}$ is the GGA exchange energy, $E_c^{LDA}$ is the LDA correlation energy, and $E_c^{nl}$ is the non-local correlation energy. The original vdW-DF (vdW-DF1) method was introduced by Dion *et al.* in 2004,[60] who used the GGA-revPBE functional for the exchange along with the LDA correlation. Later, Lee *et al.* proposed the second version, vdW-DF2, by updating both the semilocal exchange and nonlocal correlation functionals.[61] In vdW-DF2, the revPBE exchange is replaced by the reoptimization of PW86, i.e., rPW86.[62] Since both revPBE and rPW86 exchange functionals are too repulsive in a short distance range, vdW-DF and vdW-DF2 were found to lead to significant overestimations for lattice constants of metals and ionic compounds[34] as well as for adsorption energies of many molecules on metal surfaces.[63,64] Klimeš *et al.* optimized the exchange functionals (optPBE, optB88, and optB86b)[34,65] and obtained much improved results of adsorption energies.

There are tremendous ongoing efforts to optimize the exchange and non-local correlation functionals that may further improve the accuracy and efficiency of vdW-DF methods. As the traditional GGA exchange functionals are too repulsive at short distances, the revPBE in vdW-DF is replaced by softer exchange functionals from the Hartree−Fock (HF) exchange to hybrid functionals. To reduce the short-range exchange repulsion, Berland *et al.* developed a consistent exchange (cx) functional, which combines the Langereth−Vosko (LV) screened exchange and the rPW86 exchange, and Cooper constructed a $C09_x$ exchange functional by fitting the enhancement factor $F_x(s)$.[66,67] The vdW-DF-cx and vdW-DF-C09 functionals have high accuracy for the optimization of lattice constants of bulk materials and the determination of binding energies between molecules. Further, Berland *et al.* developed hybrid vdW-DF methods (e.g., hybrid-vdW-DF-cx and hydrid-vdW-DF2) by combining the Fock exchange with the vdW-DF-cx or vdW-DF2 correlation functional.[68,69] This was implemented in Quantum espresso and FHi-ABINIT codes and demonstrated high accuracy for studies of small halogenated molecules. Additionally, Vydrov and Van Voorhis derived some simple nonlocal correlation functionals, e.g., VV09,[70,71] VV10,[72] and rVV10,[73] which perform well through appropriate combinations of HF, GGA, and meta-GGA (mGGA) functionals.[74−76] For instance, the rVV10-corrected SCAN meta-GGA method (SCAN+rVV10) can accurately predict the adsorption energies and adsorption geometries of benzene on metal surfaces, better than the results obtained with vdW-DF, PBE-$vdW^{surf}$, and DFT+D methods.[74] The applicability and reliability of the DFT-$D_n$ corrections are limited by the accuracy of the system-dependent dispersion coefficients and damping functions, whereas the accuracy of the vdW-DF methods is closely related to the choice of exchange functionals. Recently, Hermann and Tkatchenko unified the two methods and developed a nonlocal many-body dispersion method (named by MBD-NL[77]) based on the VV09 nonlocal functional[78] and the Tkatchenko−Scheffler many-body dispersion model.[79] It is plausible that the MBD-NL method may reliably predict properties of many molecules, ionic and metallic compounds, and adsorbates on surfaces.

**2.3. Beyond DFT-$D_n$ and vdW-DF Methods.** Apart from the two families of popular vdW methods above, some other methods are currently also under development for the description of vdW dispersion interactions in solid and molecules, e.g., the adiabatic-connection fluctuation-dissipation theorem with the random phase approximation (ACFDF-RPA),[80] wavefunction-based approximations such as coupled cluster (CC) methods,[81] and quantum Monte Carlo (QMC) method.[82] CC and QMC methods are widely used for molecular systems, but expensive computational demands prohibit their application for large systems. In the ACFDF-RPA method, the correlation effects are directly evaluated within the ACFD framework. Then the total energy of the system can be accurately calculated through combining with the exact exchange (EXX) energy. More accurate adsorption energies of benzene on metal surfaces were obtained, comparing with results from DFT-$D_n$ and vdW-DF calculations.[83,84] Like QMC, RPA is also too expensive for handling large systems.

Recently, machine learning approaches were applied for the developments of the electronic kinetic energy functionals,[85−88] exchange-correlation functionals,[89−92] and long-range dispersion interactions.[93−97] Proppe *et al.*, proposed a DFT-D3(BJ)-GP dispersion correction method employing Gaussian process (GP) regression.[96] Based on the GGA or meta-GGA exchange and vdW correlation with the Rutgers−Chalmers approximation, Wellendorff *et al.* developed machine-learned Bayesian error estimation functional for the van der Waals correlation (BEEF-vdW/mBEEF-vdW).[93−95] They showed more accurate results of adsorption energies and structural constants than other vdW calculations (e.g., vdW-DF, optPBE-vdW, and vdW-DF2 and C09-vdW).[93−95] The transferability of machine-learned vdW functionals depends on the training datasets and still has much room to improve.

## 3. APPLICATIONS OF VDW APPROACHES FOR STUDIES OF ADSORPTION, CATALYSIS, AND TRIBOLOGY

The main purpose of this review is to assess the applicability of different vdW-DFT methods for studies of diverse physical problems, primarily with our own results. With the development of experimental techniques, the strength of vdW bonds can be quantitatively characterized with the chemical accuracy.[12] Campbell *et al.* established a database with more than 100 adsorption and reaction energies in refs 20, 99, which are useful for the validation of vdW-inclusive DFT methods. The availability of our own new experimental data such as itProbe images of vdW bonds and high-resolution (sub-millielectronvolts) molecular vibration spectra allowed us to have more stringent examinations for the accuracy of different vdW functionals.

**3.1. Molecular Adsorption Energies.** It is known that the PBE functional overestimates the adsorption energies of some simple molecules, e.g., CO and NO, but underestimates the adsorption energies of hydrocarbon molecules, e.g.,


https://dx.doi.org/10.1021/acs.jpcc.0c02293
J. Phys. Chem. C 2020, 124, 16926−16942

HCOOH and $CH_3OH$, on metal surfaces.[98,99] The long-range vdW dispersion interactions are not explicitly included in the PBE or RPBE functionals.[100] For studies of catalysis, even a small difference in adsorption energy may have a noticeable impact on the determination of reaction rates at a finite temperature; the circumstance obviously needs urgent improvements.

Benzene molecules on metal surfaces are prototypical physisorption systems and were used for benchmarking the performance of different vdW methods. Adsorption energies and geometric parameters of benzene on noble metal surfaces were extensively studied with almost all vdW functionals.[22,36,84,101−106] For example, Yildirim *et al.* found that the adsorption energy of benzene on the Ag(111) surface may change from 0.52 eV (rPW86-vdW) to 0.76 eV (optB86b-vdW), and the distance between benzene and Ag(111) also changes from 3.02 Å (optB86b-vdW) to 3.51 Å (revPBE-vdW).[106] Using normal-incidence X-ray standing wave (NIXSW) measurements, Liu *et al.* found that the adsorption height is 3.04 ± 0.02 Å for benzene on Ag(111).[14] They also determined the adsorption energies of benzene on Cu(111), Ag(111), and Au(111), e.g., 0.69 + 0.04, 0.68 + 0.05, and 0.65 + 0.04 eV, through analysis of TPD spectra based on the Polanyi−Wigner equation. Using these experimental data, they tested three vdW schemes. As shown in Figure 1, only the HSE

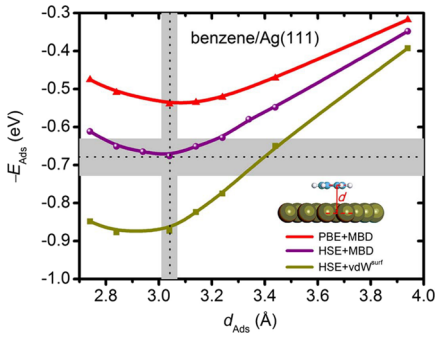


**Figure 1.** First-principles calculations for benzene on Ag(111). Binding energy $E_{ads}$ as a function of vertical distance $d_{Ads}$ of the benzene molecule center of mass from Ag(111). Calculations were carried out using three methods: semilocal Perdew−Burke−Ernzerhof (PBE) functional with many-body dispersion (MBD) interactions or hybrid Heyd−Scuseria−Ernzerhof (HSE) functional with either $vdW_{surf}$ or MBD methods for including vdW interactions. Reproduced with permission from ref 14. Copyright 2015 American Physical Society.

+MBD method can give both correct adsorption energy and adsorption height for benzene on Ag(111). Campbell *et al.* reanalyzed these TPD data using a better prefactor for desorption and reported slightly different adsorption energies for benzene on noble metal surfaces,[18] e.g., 0.72 eV on Au(111), 0.68 eV on Cu(111), and 0.63 eV on Ag(111). Nonetheless, the best fit is still provided by the HSE+MBD method.

We expanded the scope by combining vdW-inclusive DFT calculations with milliKelvin STM measurements of single benzene molecules on the Ag(110) substrate.[22] As shown in Table 1, all vdW functionals employed in our calculations yield the largest adsorption energy for the short bridge geometry on the Ag(110) surface, in agreement with the experimental result. It is not a surprise that plain GGA-PBE calculations produce an unreasonably low adsorption energy and large height of benzene on the Ag surface. RevPBE-vdW and rPW86-vdW functionals tend to underestimate the adsorption energy, while the DFT-D2 method overestimates the adsorption energy. The improved DFT-$D_n$ methods and optimized vdW-DF functionals appear to give reasonable results for this system, in comparison with the corresponding experimental data.

In Figure 2, we show that PW91, PBE, and RPBE calculations give large errors for adsorption energies comparing with the SCAC data. For chemisorption systems, the BEEF-vdW approach can indeed improve adsorption energies. However, for adsorbates with weak interactions, the BEEF-vdW method fails to reach the chemical accuracy as required for catalysis studies.[98] Sautet *et al.* tested several vdW functionals (optPBE-vdW, optB86b-vdW, BEEF-vdW, and PBE-dDsC) through studying adsorbates such as ethylene, cyclohexene, benzene, naphthalene, CO, $O_2$, $H_2$, methane, and ethane on Pt(111).[101] Figure 3 compares 39 adsorption energies of different common catalytic intermediates on transition-metal surfaces; the lowest mean absolute deviations (MADs) away for the corresponding experimental data are obtained with the optPBE-vdW and PBE-dDsC functionals (0.2 eV), while PBE and optB86b-vdW give two times larger MADs (∼0.45 eV). BEEF-vdW is in the middle, with a MAD of 0.33 eV. For laterally p-bound unsaturated hydrocarbons (cyclohexene, benzene, and naphthalene), the PBE and BEEF-vdW functionals are severally underbound, while optPBE-vdW and PBE-dDsC provide good matches with experiments. Recently, Hensley *et al.* developed a simple method for predicting adsorption energies using an adaptively weighted sum of energies from RPBE and optB86b-vdW (or optB88-vdW) functionals.[107] They calculated adsorption energies of 39 cases and found that this method gives MADs of 0.14 and 0.2 eV, smaller than 0.21 and 0.27 eV with the BEEF-vdW functional. For systems with large vdW contributions, this method reduces MADs to 0.12 and 0.18 eV, respectively.

Recently, we assessed the performance of 14 different vdW methods on predicting the adsorption properties of formic acid (HCOOH) and formate (HCOO) molecules on the Pt(111) surface.[63] As shown in Figure 4, the adsorption energies of HCOOH/HCOO on Pt(111) can be determined with high accuracy using the improved vdW correction methods (e.g., PBE+D3, PBE+D3-BJ, PBE+dDsC, PBE+TS, PBE+TS-SCS, and PBE+TS/IH), many-body dispersion method (PBE +MBD@rsSCS), and the optimized vdW functional methods (e.g., optPBE-vdW, optB88-vdW, and optB86b-vdW). Comparing to the SCAC data by Campbell *et al.*,[19] the MADs of HCOOH's or HCOO's adsorption energies using these 10 vdW methods can be as small as 0.05−0.09 eV.

Converting $CO_2$ to methanol or higher alcohols through multiple hydrogenation steps on metal catalysts is an attractive topic for solving the energy and environmental issues. Trapping $CO_2$ molecules is the onset of these reactions. The adsorption energy of $CO_2$ is typically underestimated in most DFT calculations and the inclusion of vdW correction is essential. Muttaqien and co-workers[108] studied the adsorption of $CO_2$ on Cu surfaces using the van der Waals density functionals (vdW-DFs), i.e., the original vdW-DF (vdW-DF1), optB86b-vdW, and rev-vdW-DF2[109] as well as the PBE with dispersion correction (PBE-D2). They found that vdW-DF1 and rev-vdW-DF2 functionals underestimate the adsorption energy, while PBE-D2 and optB86-vdW functionals give better


https://dx.doi.org/10.1021/acs.jpcc.0c02293
J. Phys. Chem. C 2020, 124, 16926−16942

**Table 1. Energies of the Six External Vibrational Modes (in meV), Adsorption Energy ($E_{ad}$, in eV), and the Shortest Perpendicular Distance Separating the Carbon and Ag Atoms ($d_{C-M}$, in Å) for Benzene Adsorbed on the Ag(110) Surface**

| vdW functionals | $FR_x$ | $FR_y$ | $FR_z$ | $FT_x$ | $FT_y$ | $FT_z$ | $E_{ad}$ | $d_{C-M}$ |
|---|---|---|---|---|---|---|---|---|
| GGA-PBE | 6.4 | 3.3 | | | 1.4 | 4.2 | −0.121 | 3.06 |
| revPBE-vdW | 8.9 | 5.6 | 1.4 | | 2.4 | 6.3 | −0.523 | 3.07 |
| rPW86-vdW | 9.8 | 5.3 | 2.6 | 1.4 | 2.8 | 7.1 | −0.519 | 3.04 |
| optPBE-vdW | 11.3 | 6.2 | 1.3 | | 3.4 | 8.1 | −0.718 | 2.80 |
| optB88-vdW | 14.4 | 6.7 | 0.3 | | 4.3 | 9.7 | −0.805 | 2.69 |
| optB86b-vdW | 14.5 | 7.2 | 2.3 | | 4.6 | 10.3 | −0.851 | 2.61 |
| DFT-D2 | 16.6 | 9.8 | 1.7 | | 4.6 | 11.6 | −0.970 | 2.56 |
| DFT-D3 | 12.3 | 7.4 | 1.9 | | 3.2 | 8.9 | −0.781 | 2.77 |
| DFT-D3(BJ) | 15.0 | 8.3 | 2.0 | | 4.0 | 11.4 | −0.861 | 2.71 |
| DFT-TS | 12.1 | 8.5 | 1.1 | | 4.3 | 9.0 | −0.840 | 2.71 |
| DFT-TS+SCS | 13.0 | 8.2 | 2.0 | | 3.5 | 9.4 | −0.937 | 2.74 |

Reproduced with permission from ref 22. Copyright 2017 ACS Publications.

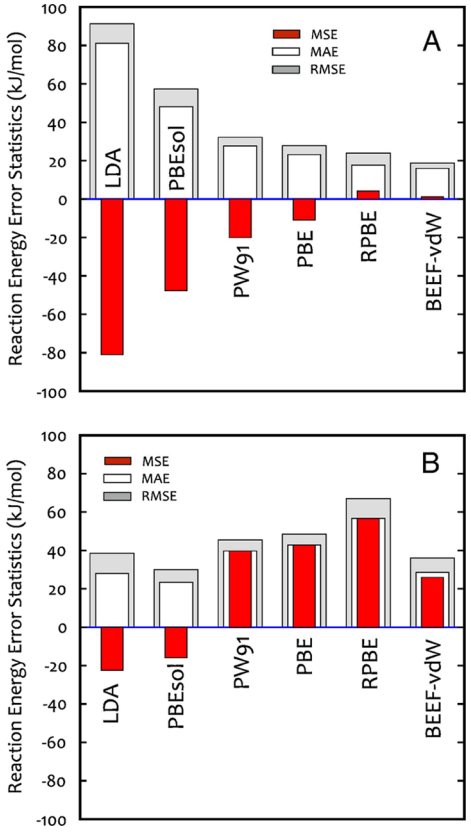


**Figure 2.** Comparison of the accuracy of the different density functionals relative to the experimental data for two different data sets: (A) purely chemisorbed systems where van der Waals (vdW) interactions contribute little to the adsorption energy and (B) systems where vdW interactions are thought to contribute a large amount to the adsorption energy. Reproduced with permission from ref 98. Copyright 2015 Elsevier.

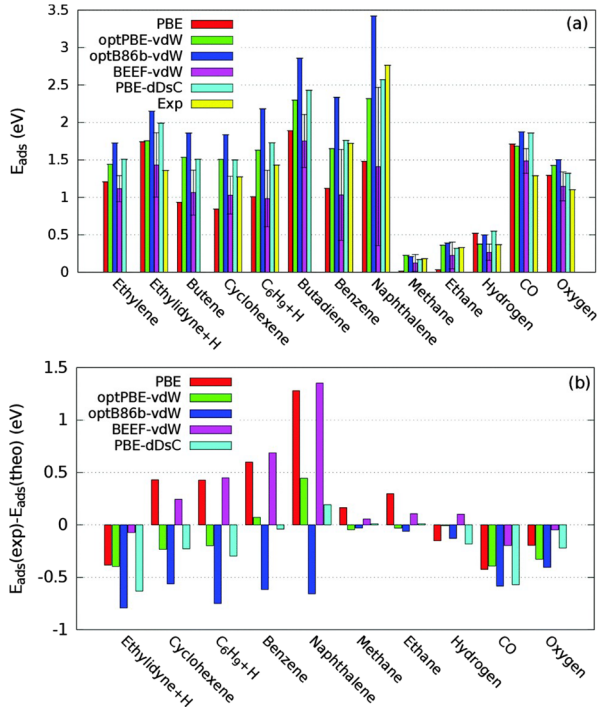


**Figure 3.** (a) Adsorption energy (eV) on Pt(111) at 1/9 ML for the considered systems, calculated with the five considered functionals. The experimental value (see text for the evaluation method) is indicated in yellow when available. (b) Adsorption energy deviation between experimental data and calculated results for the studied systems on Pt(111) for the five considered functionals. Reproduced with permission from ref 101. Copyright 2015 The Royal Society of Chemistry.

agreement with the experimental estimate for the adsorption energy of $CO_2$ on Cu(111) (Figure 5).

Obviously, current vdW-inclusive DFT methods are still not satisfactory for the description of vdW interactions in physisorption systems, even for adsorption energies and adsorption geometries, which are probably the simplest outcomes of DFT calculations.[110−112] The applicability and accuracy of different vdW methods still need extensive tests and analyses. One outstanding example is the incorrect adsorption geometry of CO on Pt given by DFT optimizations, which was traced to the correlation effect on the antibonding orbitals of CO.[113] Benchmark calculations and experimental data of molecular adsorption geometries and energies are undoubtedly needed for the further development of more accurate and universal vdW-inclusive DFT methods.

**3.2. Molecular Vibrational Energies.** According to the harmonic transition state theory (HTST), the rate constants of many catalytic reactions are closely related to vibrational frequencies of reactants.[114−116] For physisorption systems with vdW interactions, such as benzene or hydrogen molecule on coinage metal surfaces, how to determine the vibrational frequencies is a challenging task. Furthermore, the low energy external vibration modes are more sensitive to a slight change


https://dx.doi.org/10.1021/acs.jpcc.0c02293
J. Phys. Chem. C 2020, 124, 16926−16942

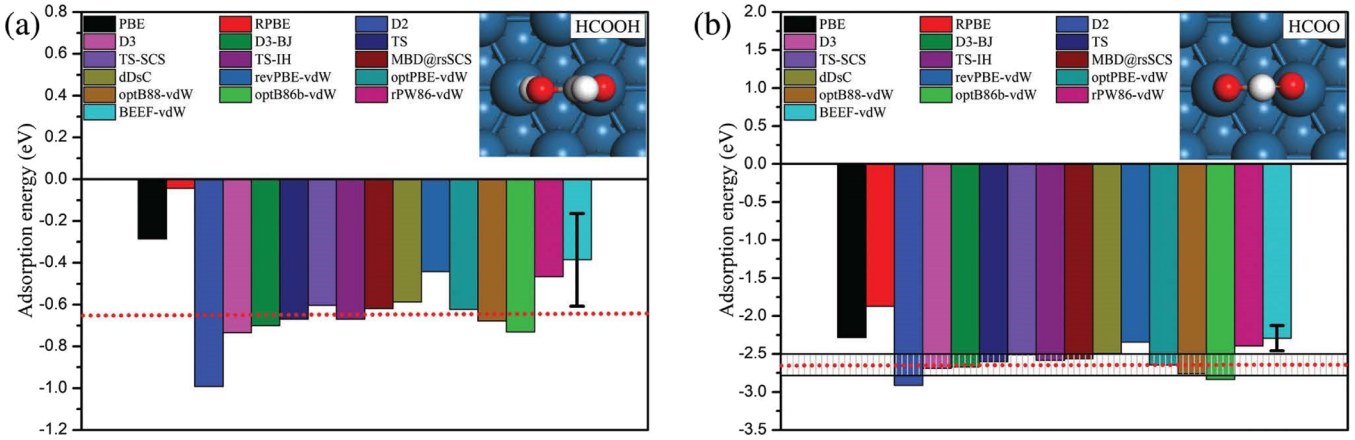


**Figure 4.** Adsorption energy of (a) HCOOH and (b) HCOO on the Pt(111) surface at 1/4 monolayer (ML) coverage calculated with GGA functionals (PBE and RPBE) and 14 vdW-inclusive density functional theory methods. The estimated error bars of BEEF-vdW are 0.222 and 0.179 eV for HCOOH and HCOO, respectively. The experimental value (−0.65 eV) of HCOOH adsorption energy is given by the horizontal dotted line in (a). The horizontal dotted and solid lines represent the experimental value (2.63 ± 0.13 eV) that included experimental errors of the bidentate HCOO adsorption energy in (b). The experimental values were obtained by SCAC measurements.[19] The insertions are the adsorption configurations of HCOOH and HCOO on the Pt(111) surface. Reproduced with permission from ref 63. Copyright 2019 The Royal Society of Chemistry.

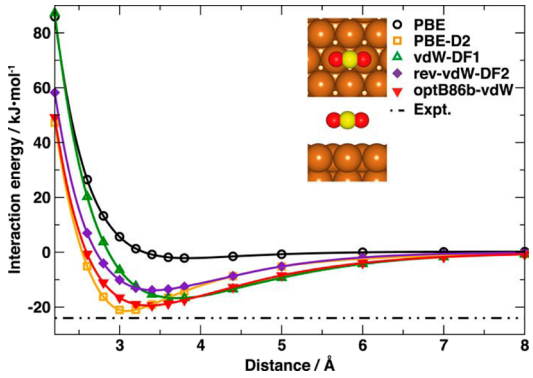


**Figure 5.** Interaction energy ($E_{int}$) curve of $CO_2$ on Cu(111) as a function of molecule−surface distance. Insets show the top and side views of $CO_2$ adsorption on the bridge site of Cu(111). The horizontal dashed-dotted line indicates the estimated desorption energy from TPD of $CO_2$ on Cu(111) at a low coverage Reproduced with permission from ref 108. Copyright 2017 AIP Publishing.

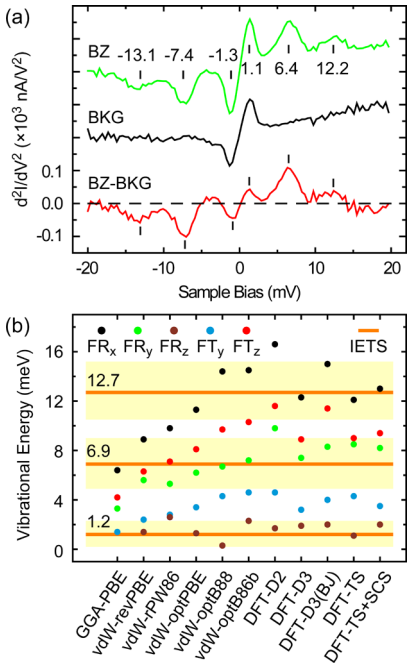


**Figure 6.** Analysis of a single benzene molecule on Ag(110). (a) STM-IETS vibrational spectroscopy at 600 mK measured with a bare metal tip: over the molecule (top curve in green), Ag surface (background, middle curve in black), and background-subtracted spectrum (bottom curve in red). Taking the average value of the peak and dip energy positions as the vibrational excitation energy: 1.2, 6.9, and 12.7 mV. (b) Comparison of calculated external vibrational modes with STM-IETS measurement for benzene adsorbed on Ag(110) Reproduced with permission from ref 22. Copyright 2017 ACS Publications.

of vdW bonds between adsorbates and substrates and they hence provide a much more stringent means for benchmarking vdW functionals than the adsorption energies.

We systematically studied the low-energy external vibration modes of benzene on the Ag(110) surface by combining the milliKelvin STM measurements and vdW-inclusive DFT calculations.[22] Sub-Kelvin itProbe and STM-IETS enable accurate determination of adsorption site, structure, and external vibration frequencies at the single-molecule level. From STM-IETS measurements, three vibrational excitation energies at 1.2, 6.9, and 12.7 mV were found (see Figure 6), which were attributed to the external vibrational modes of benzene on Ag. We used 10 different vdW-inclusive approaches (revPBE-vdW, rPW86-vdW, optPBE-vdW, optB88-vdW, optB86b-vdW, DFT-D2, DFT-D3, DFT-D3(BJ), DFT-TS, and DFT-TS+SCS) so as to test their applicability for the description of the external vibrational modes that unveil the weak bonds between benzene and Ag. All vdW functionals correctly produce the ground-state adsorption geometry, with the center of the benzene ring on top of the short bridge site of Ag(110). However, they give rather divergent vibrational energies of external modes. Compared with data from STM-IETS measurements (see Figure 6), the optimized vdW functionals (optPBE, optB88, and optB86b) and improved dispersion-corrected vdW methods (DFT- D3) are among the best for getting good


https://dx.doi.org/10.1021/acs.jpcc.0c02293
J. Phys. Chem. C 2020, 124, 16926−16942

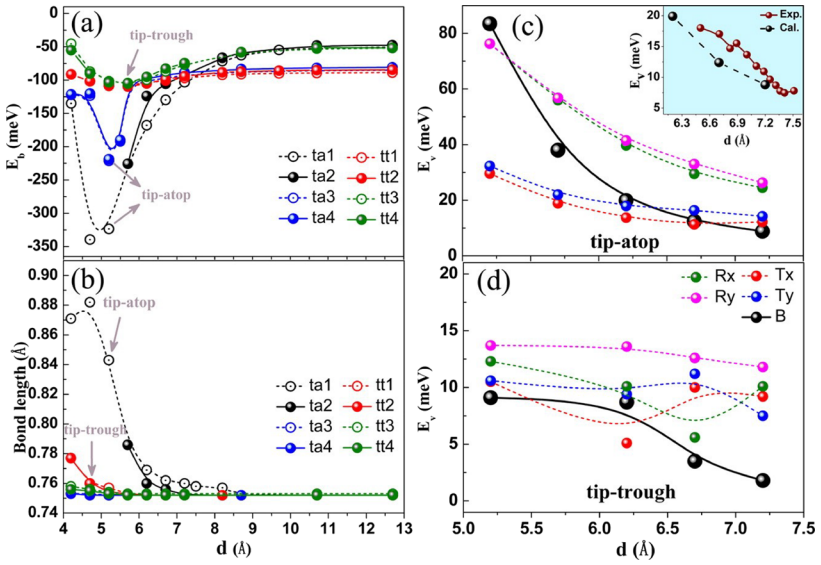


**Figure 7.** (a) Binding energy and (b) bond length versus variation of the tip−substrate distance for the $H_2$ molecule at different adsorption sites. Vibrational energies, $E_v$, versus tip−substrate distance for the $H_2$ molecule adsorbed in (c) tip-atop junction and (d) tip-trough junction. The inset in (c) shows the experimental vibrational energies for the tip−substrate distance in the range from 6.5 to 7.5 Å that can be directly compared to the calculated results. Reproduced with permission from ref 117. Copyright 2015 ACS Publications.

frequencies of all three low-energy vibrational modes. We also investigated the properties of a single $H_2$ molecule trapped in nanocavities with controlled shape and separation between the STM tip and the missing-row Au (110) surface.[117] Again, the optB86b-vdW functional appears to give reliable results for the bond length and rotational and vibrational energies of $H_2$ (see experimental and theoretical results in Figure 7 for the tip−substrate distance in the range from 6.5−7.5 Å).

The study of intermolecular coupled vibrations has played an important role in the understanding of catalytic reactions,[118] particularly those in the artificial environment set by STM or AFM tips.[119,120] We detected an intermolecular coupled vibration mode between two CO molecules: one on the surface and the other on the STM tip within the gap of a sub-Kelvin STM. This new vibrational mode (about 7 meV) emerges as the gap shrinks and two CO molecules strongly interact in the junction. The vdW-corrected DFT method (DFT-D3) can capture the individual and coupled vibrational modes well (see Figure 8).

Yoon *et al.* studied the contribution of vibrational energies to free energies of $H_2$ on metalloporphyrin-incorporated graphene using LDA, GGA, and vdW functionals.[121] For weak adsorptions, the zero-point energy and vibrational free energy significantly depend on the choice of vdW functionals (see Figure 9). For the Zn case, the difference of vibrational free energy of adsorbed $H_2$ is *ca.* 0.05 eV between vdW-DF (revPBE-vdW)/vdW-DF2 (rPW86-vdW) and PBE+TS (see Figure 9). Again, these results suggest that the present vdW approaches are still not satisfactory for catalysis studies.

**3.3. Catalytic Activity and Selectivity.** The activity and selectivity of heterogeneous catalysts sensitively depend on the energy barriers along different pathways. One may note the huge increase in DFT studies for various catalysis processes with the availability of vdW functionals.[1,5,33,38,122−126] As discussed above, the choice of vdW-inclusive DFT methods has an important influence in the reliable determination of adsorption geometries, energies, and vibration frequencies and

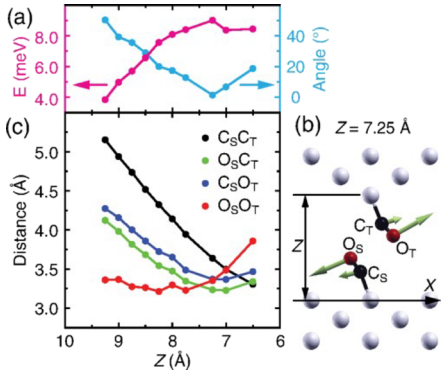


**Figure 8.** (a) Calculated energy of coupled vibrational mode (magenta curve) and the angle (light blue curve) versus tip−sample distance $Z$. The energy reaches a maximum at $Z$ = 7.25 Å. (b) Schematic diagram of the coupled mode eigenvector at $Z$ = 7.25 Å; $Z$ is defined as the vertical distance from the protruding Ag atom on the tip and the Ag surface layer before structure relaxation in the calculation. (c) $Z$ dependence of distances between pairs of atoms in the two CO molecules. Reproduced with permission from ref 120. Copyright 2017 APS Publications.

hence may affect the design strategies. Here, we select a few examples to comment on the current status of the field.

For the dissociation of small molecules ($H_2$, $N_2$, and $CH_4$), Kroes *et al.* analyzed the effect of the choosing different DFT functionals on results of their potential energy surfaces and reaction dynamics on the Ru, Ni, Pt, and Cu surfaces.[127,128] These functionals include vdW-DF, vdW-DF2, and revTPSS meta-GGA. It shows that the vdW-DF and vdW-DF2 functionals reproduce a correct reaction pathway as observed in molecular beam experiments for $H_2$ and $D_2$. In this aspect, the BEEF-vdW method was found to give reasonable energy barrier heights within an error bar of 0.14 eV compared to experimental values for dissociation reactions of these small molecules.[127,128]

Illas *et al.* studied the effect of vdW interactions on the potential maps and reaction rates of the water-gas shift reaction


https://dx.doi.org/10.1021/acs.jpcc.0c02293
J. Phys. Chem. C 2020, 124, 16926−16942

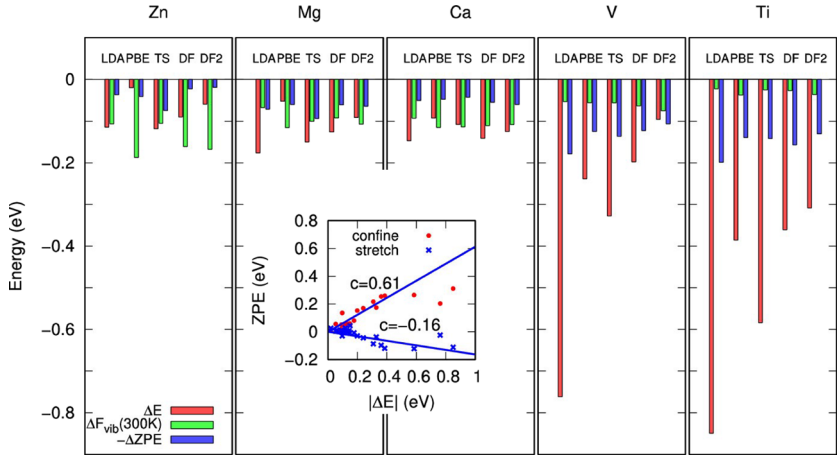


**Figure 9.** Decompositions of chemical potential into binding energy ($\Delta E$), entropic free energy ($\Delta F_{vib}$), and ZPE change ($\Delta$ZPE). Inset shows the linear relation between the absolute values of binding energy and the confinement part and stretch part of ZPE for weak binding systems. Reproduced with permission from ref 121. Copyright 2018 ACS Publications.

on the Cu(321) surface.[5] They found that the inclusion of dispersion terms in calculations does not change the qualitative picture of the overall reaction, maintaining the rate-determining step and the predominant route. In contrast, in the OH + OH → $H_2O$ + O reaction, the dispersion effect may alter reaction rates by up to three orders of magnitude; the formation of carboxyl is unfavored when dispersion terms are explicitly included. Furthermore, the reaction rate for $CO_2$ production (at 463 K) through *cis*-COOH dissociation may also alter by three orders of magnitude by including dispersion terms in calculations for the energy barrier.

Methanol, ethanol, ethylene glycol, formic acid, propanol, and glucose are important fuels for direct alcohol fuel cells.[129] The dispersion interaction plays a vital role to the adsorption geometries and energies of these molecules on anodic catalysts of fuel cells. Particularly, in the alcohol dehydrogenation reactions, inclusion of vdW interactions is extremely important for the determination of adsorption energies of adsorbates and reaction intermediates, which govern the activity and selectivity of C−H and O−H bond breaking. The decomposition pathways of HCOOH on metal surfaces have been extensively studied, which provide some fundamental understanding about the HCOOH electrooxidation in direct formic acid fuel cells.[130−135] This decomposition process follows two reaction pathways: HCOOH → $CO_2$ + $H_2$ ($CO_2$ pathway) and HCOOH → CO + $H_2O$ (CO pathway). HCOO is a key intermediate in the $CO_2$ pathway, which is formed by cleaving the O−H bond of HCOOH. However, the C−H cleavage results in the formation of COOH, which further leads to a poisoning product of CO via the COOH → CO + OH reaction. Therefore, the reliability of activation barriers for O−H and C−H bond breaking are crucial for the theoretical determination of catalytic selectivity of a catalyst toward HCOOH's decomposition, even before giving correct predictions of reaction rates. For the latter, an error of only 0.21 eV in the adsorption energy for the adsorbed intermediate or transition state may cause a change of the reaction rate by over 400-fold at 400 K.[12] Putra *et al.* studied the adsorption and decomposition mechanisms of monomeric formic acid (HCOOH) on a Cu(111) surface using several DFT functionals (PBE, PBE-D2, and vdW-DFs).[134] They found that the activation energies for the decomposition of HCOOH from PBE-D2 and vdW-DFs calculations are lower than desorption energies, seemingly in contradiction with experimental findings that indicate no HCOOH decomposition on Cu(111) when the surface is exposed to the gas-phase HCOOH at room temperature. The calculated activation energies of HCOOH decomposition on Cu(111) with the zero point energy (ZPE) correction are 0.37, 0.31, 0.32, and 0.30 eV with the PBE, PBE-D2, rev-vdW-DF2, and optB86b-vdW functionals, respectively. The deviations for this case appear to be not large (see Figure 10).

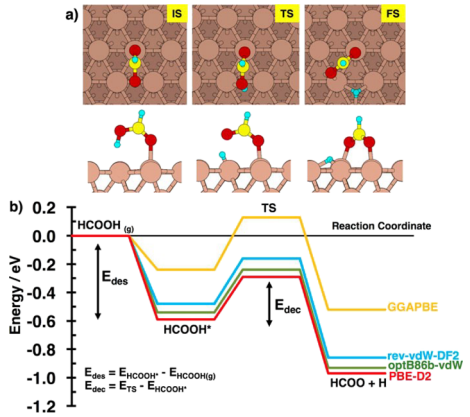


**Figure 10.** (a) Decomposition process of the OH-perpendicular configuration. IS, TS, and FS represent the initial state, transition state, and final state, respectively. (b) Energy profile for the OH-perpendicular configuration decomposition on Cu(111). Reproduced with permission from ref 134. Copyright 2019 AIP Publications.

Recently, we studied the adsorption and catalytic dehydrogenation of HCOOH on the Pt(111) surface using different vdW-inclusive DFT methods.[63] Our results indicate that the PBE+dDsC method has the best overall performance on the description of adsorption and catalytic selectivity. We found that the improved vdW-corrected methods (PBE+D3, PBE+TS, PBE+TSSCS, PBE+TS/IH, PBE+MBD@rsSCS, and PBE+dDsC) and optimized vdW functionals (optPBE-vdW, optB88-vdW, and optB86b-vdW) perform well to estimate the adsorption energies of HCOOH and HCOO molecules on the Pt(111) surface. The vdW-inclusive DFT approaches and the conventional PBE functional predict a higher activation barrier


https://dx.doi.org/10.1021/acs.jpcc.0c02293
J. Phys. Chem. C 2020, 124, 16926−16942

for C−H bond breaking than O−H bond breaking in the dehydrogenation of formic acid. However, the optimized vdW functionals evidently overestimated the barrier difference for C−H breaking and O−H breaking (see Figure 11) and then

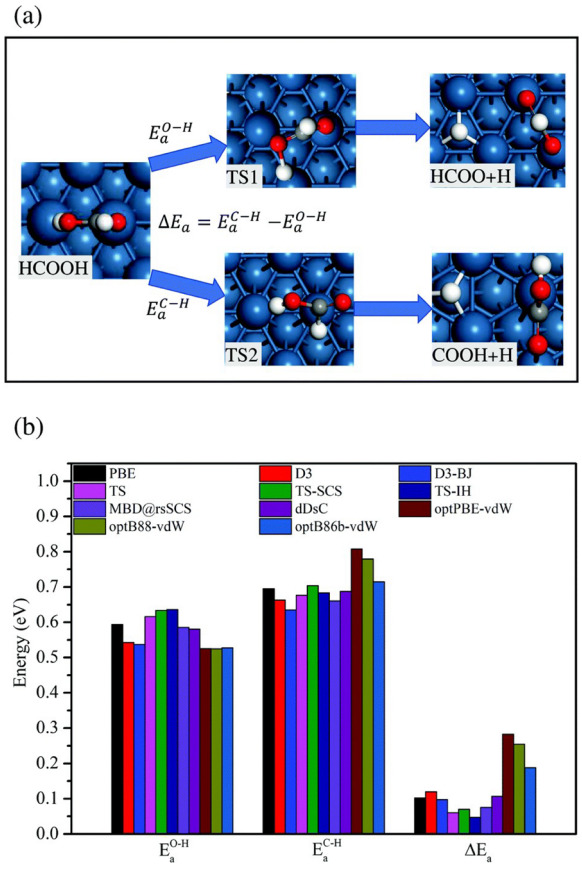


**Figure 11.** (a) Geometries of adsorbates in HCOOH → HCOO + H and HCOOH → COOH + H reactions on the Pt(111) surface. (b) Comparison of the calculated barriers ($E_a^{O-H}$ and $E_a^{C-H}$) in the two dehydrogenation pathways using the PBE functional and 10 vdW methods. The difference of two barriers ($\Delta E_a = E_a^{C-H} - E_a^{O-H}$) is given. Reproduced with permission from ref 63. Copyright 2019 The Royal Society of Chemistry.

underestimate the rate constant of the C−H bond breaking reaction, which fails to describe the catalytic selectivity of HCOOH's dehydrogenation (see Figure 12). Both PBE+dDsC and PBE predict a similar temperature dependence of reaction rates for O−H breaking versus C−H breaking (see Figure 12).

Direct methanol fuel cells are ideal power sources for small devices such as cellular phones and laptops since they have low operating temperatures, 50−120 °C, and no requirement for a fuel reformer. The oxidation of methanol to hydrogen ions and carbon dioxide on anodes $CH_3OH + H_2O \rightarrow CO_2 + 6H^+ + 6e^-$ requires highly efficient catalysts. The methanol dehydrogenation starts from cleavage of the O−H and C−H bond as $CH_3OH \rightarrow CH_3O \rightarrow CH_2O \rightarrow CHO \rightarrow CO$ and $CH_3OH \rightarrow CH_2OH \rightarrow CHOH \rightarrow COH \rightarrow CO$ pathways.[136] Pham *et al.* studied the effects of the dispersion interaction on the equilibrium structure of adsorbed methanol and the energetics of methanol decomposition via the C−H and O−H bond scissions on Pt(111) with PBE and optB86b-vdW functionals.[126] The DFT results show that the dispersion interaction significantly reduces the equilibrium distance and

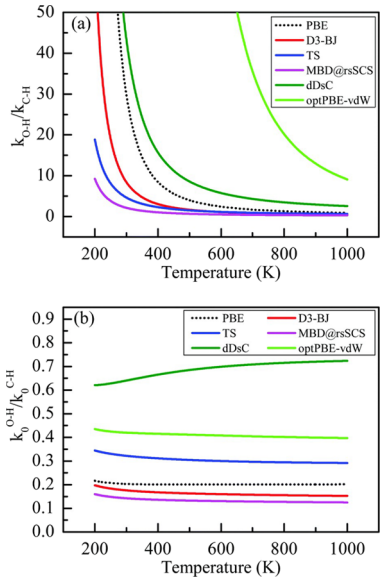


**Figure 12.** Temperature dependence of the ratio of (a) reaction rate constants and (b) prefactors of Arrhenius expression for O−H breaking versus C−H breaking in HCOOH's dehydrogenation process. Reproduced with permission from ref 63. Copyright 2019 The Royal Society of Chemistry.

increases the adsorption energy of methanol on the top site of Pt(111) to 0.63 eV, thereby making it closely in accord with the experimental result (0.58 eV).[18] Comparing to the PBE functional, the optB86b-vdW functional demonstrates that the dispersion interaction facilitates methanol decomposition via the C−H bond scission (see Figure 13).

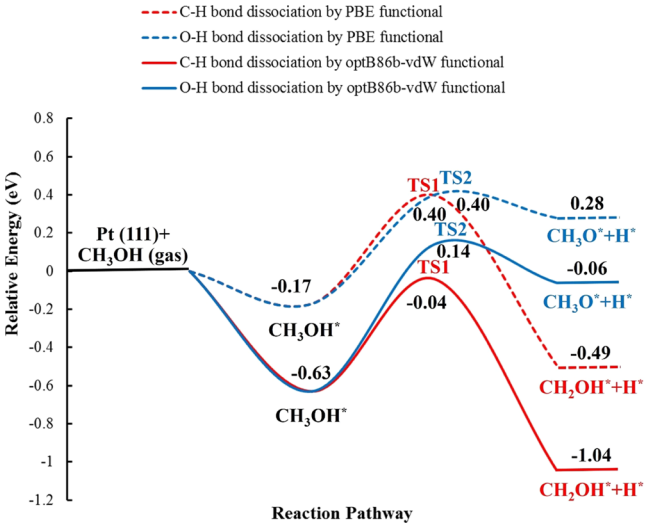


**Figure 13.** Potential energy surface for $CH_3OH$ decomposition via the C−H and O−H bond scissions on Pt(111). Reproduced with permission from ref 126. Copyright 2019 Elsevier.

Chen *et al.* used the PBE+TS method to investigate the potential energy paths of methanol, ethanol, 1-propanol, and 1-butanol dehydrogenation on Cu(110).[110−112] They found that the DFT-TS correction improves the description of the interaction between methanol and Cu than the vdW-DF2 correction. However, in comparison with a previous non-vdW study of methanol decomposition, the kinetic barriers of


https://dx.doi.org/10.1021/acs.jpcc.0c02293
J. Phys. Chem. C 2020, 124, 16926−16942

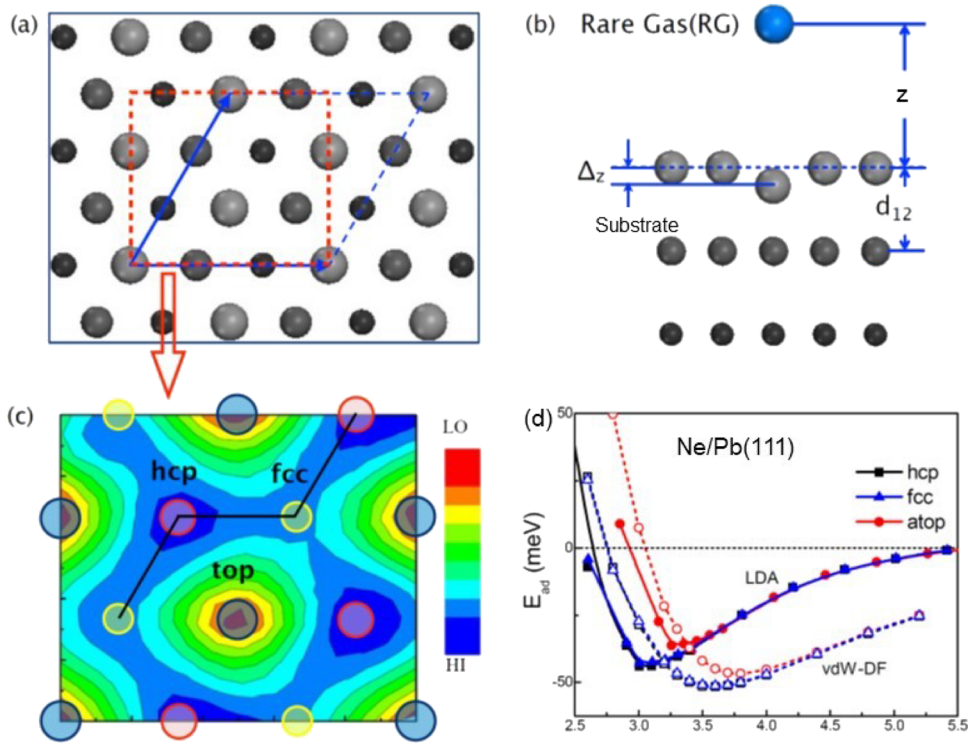


**Figure 14.** Panels (a) and (b) are top and side views of the atomic model adopted in the related calculations, respectively. Parallelogram and rectangle in (a) show the $\sqrt{3}x\sqrt{3}$ unit cell and the "mapping" region displayed in panel (c), respectively. The large, medium, and small spheres are for the surface, subsurface, and third layer atoms, and notations $z$ and $\Delta_z$ are marked for the convenience of discussion. (c) Contours of the $E_{ad}$ of Ne/Pb(111) using LDA. (d) Position- and distance-dependent $E_{ad}$ of Ne/Pb(111). Solid and open symbols represent results from the LDA and vdW-DF using the optB86b exchange term, respectively. Reproduced with permission from ref 149. Copyright 2011 APS Publications.

methanol dehydrogenation are not significantly changed, in part due to the fact that vdW interactions contribute to initial, final, and transition states almost equally.

In view of the progresses made in catalysis studies using the vdW-inclusive DFT methods, the current schemes still have noticeable discrepancies for adsorption energies and activation energies in most cases. The improved vdW corrected methods, e.g., DFT+D3, DFT+TS, DFT+TS-SCS, DFT+TS/IH, MBD@rsSCS, and DFT+dDsC) and optimized vdW functionals (optPBE-vdW, optB88-vdW, and optB86b-vdW) can already give acceptable results. A more difficult challenge is for the calculation of vibration frequencies as the vibrational entropy term is important for the determination of reaction rates and even for the identification of reaction pathways.

**3.4. Adsorption and Tribological Features of Rare Gas Atoms on Solid Surfaces.** Theoretical studies of tribology, aiming at the development of clear microscopic understandings on friction and wear, have touched on various effects such as electron−hole pair excitations, chemical reactions, and dynamics of defect creation and diffusion.[137−143] Rare gas (RG) are frequently used in modeling systems for studies of tribological properties. Figure 14a,b displays an RG layer in an ordered $(\sqrt{3}\times\sqrt{3})$R30° pattern on the close-packed metal surfaces, as typically observed for these systems by the low-energy electron diffraction measurements.[28,144] DFT calculations may produce position-dependent adsorption energies as the RG layer slides along different pathways on the substrate, i.e., the potential energy surfaces (PESs), for quantitative analysis of tribological properties. As a rule of thumb, systems with strongly corrugated PESs have high friction and vice versa.

It was found that LDA and GGA functionals gave inconsistent descriptions for the adsorption structures and the energetics of RG−metal systems,[145−149] and the inclusion of nonlocal vdW correction is critical for the correct determination of their adsorption and friction features.[150,151] We calculated adsorption energies of RG/Pb(111) by using the optB86b functional,[34,60,152,153] which noticeably changes the adsorption energies and adsorption heights for Ne/Pb(111) as shown in Figure 14d. Quantitatively, the calculated $E_{ad}$ of Xe/Pb(111), 173 meV, is very close to the experimental value, 191 ± 10 meV,[150] demonstrating the reliability and limitation of the current vdW functionals for theoretical studies in this subfield. The PES map in Figure 14c shows that both Ne and Kr prefer the high-coordination hcp-hollow site of Pb(111) and disfavor the low-coordination atop site. The energy differences between the atop and hcp adsorption geometries for Ne/Pb(111) and Kr/Pb(111) are 4.8 and 9.8 meV, respectively. As a result of a more corrugated PES, the motion of Kr on Pb(111) is essentially blocked at 5 K while Ne is still mobile. As corrugations of PESs are at the millielectron-volt level, tribological properties of RG layers also provide useful testing cases to examine the accuracy of different vdW functionals. We also noted that a large energy cutoff for basis expansion (e.g., 600−800 eV for plane waves) is important for the numerical convergence.

Chen *et al.* compared the calculated adsorption energy, equilibrium distance, and vibrational energy of noble gases (Kr and Xe) on various metal surfaces at low-coordination sites obtained by LDA, PBE, and vdW-DF2 methods (see Table 1 in ref 154. They demonstrated the importance of nonlocal vdW for obtaining results in quantitative agreement with


https://dx.doi.org/10.1021/acs.jpcc.0c02293
J. Phys. Chem. C 2020, 124, 16926−16942

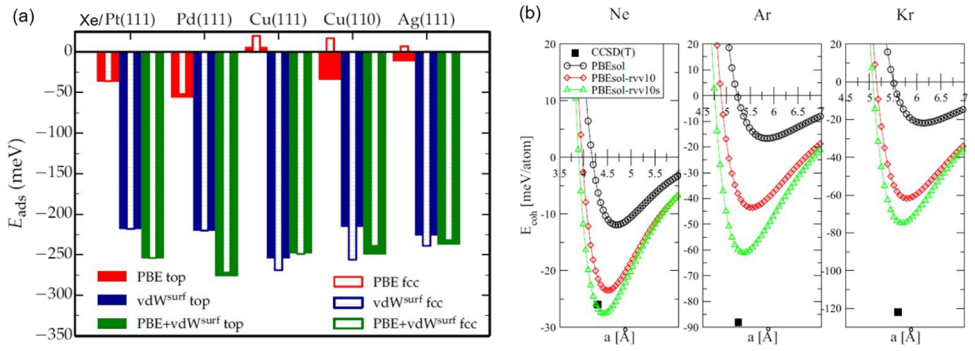


**Figure 15.** (a) Adsorption energies $E_{ads}$ calculated with PBE+vdW$^{surf}$ for Xe on transition-metal surfaces.[162] (b) Cohesive energy curves versus lattice constant for Ne, Ar, and Kr obtained from the PBEsol, PBEsol+rVV10, and PBEsol+rvv10s functionals, respectively.[163] Reproduced with permission from refs 164, 165. Copyright 2016 APS Publications and 2018 APS Publications, respectively.

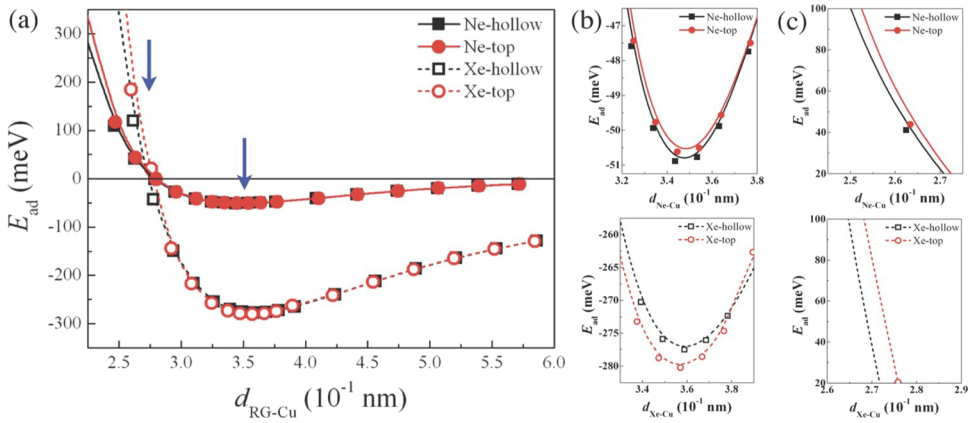


**Figure 16.** Position- and distance-dependent adsorption energies of Ne (solid symbols) and Xe (open symbols) on Cu(111). Squares and circles are for energies of RG adatoms on hollow and top sites, respectively. The solid and dashed lines are for eye-guiding purpose. Panels (b) and (c) show the zoom-in plots at the negative and positive adsorption energy regions, as highlighted by the arrows in (a), respectively. Reproduced with permission from ref 155. Copyright 2014 APS Publications.

experiments. Theoretical studies of RG/Cu(111) showed that different vdW versions[147,155,156] are reasonably consistent and provide significant improvements over LDA results. Our own calculations for Xe on Cu(111) are also consistent with previous calculations[155,156] and agree well with experiments.[157] The estimated sliding temperature for Xe/Cu(111) from the corrugation of PES is at about 35 K, which is very close to the experimental result of 50 K by Mistura *et al.* using the quartz microbalance technique under a high vacuum condition.[155] Silvestrelli *et al.* further invoked the screening effect[158,159] and studied the adsorption of Xe and graphene on Ni(111)[160] and other noble metal surfaces.[161] Ruiz *et al.* modeled screened vdW interactions for atoms/molecules on surfaces (the so-called DFT+vdW$^{surf}$ method)[162] and found that the calculated adsorption energies are in the right range of experimental results. As displayed in Figure 15a, the top and fcc adsorption sites are virtually degenerate in the case of Xe/Cu(111), and the PBE contribution destabilizes the fcc hollow adsorption site upon relaxation with obvious positive values. By adding density-gradient dependence in the expression of rVV10 nonlocal vdW correction, Terentjev *et al.* recently developed a new dispersion-corrected functional of PBEsol+rVV10s using plane waves[163] or atomic orbitals.[164] As shown in Figure 15b, the PBEsol+rVV10s functional was found to be more reliable for the determination of cohesive energies than the PBEsol or PBEsol+rVV10 functional in the region near equilibrium, and the calculated adsorption energies are in close agreement with experiments (cf. Table V in ref 163).

It is also interesting to analyze the change of PES as the RG−surface distance is shortened for the understanding of tribological properties as lubricant interfaces are typically under a pressure.[165−168] Using the adsorption of Ne and Xe on Cu(111) in Figure 16a as an example, the lowest energy on the PES of Ne/Cu(111) is on the hollow site around the equilibrium region in Figure 16b, while that of Xe/Cu(111) is on the atop site. The opposite PES features of Ne and Xe on Cu(111) disappear in the repulsive part in Figure 16c if we zoom in the plots to an energy range of ∼20−100 meV that are used in typical helium atom scattering (HAS) experiments.[165] The detailed analyses of projected density of states of both systems illustrated that Xe-Cu(Au) p-d hybridization is the main reason for the preference of the atop site around the equilibrium distance,[155] even though it is perceived that RG atoms interact only via the vdW forces with substrates. Note that the PES of Xe/Cu(111) in Figure 16a (also in Figure 17a) undergoes a transition of favorite adsorption sites from the atop site to the hollow site at two "critical" RG−substrate distances, $Z_c$ = 2.9 and 3.8 Å.[169] Analogously, we found the potential crossings at $Z_c$ = 3.52 Å for Xe/Pd(111) and $Z_c$ = 4.05 Å for Ar/Cu(111) in the far-surface regions. At these critical distances, the friction collapses and a superlubric state can be realized under a low compression or stretch due to the electrostatic repulsion-driven flattening of PESs. This should


https://dx.doi.org/10.1021/acs.jpcc.0c02293
J. Phys. Chem. C 2020, 124, 16926−16942

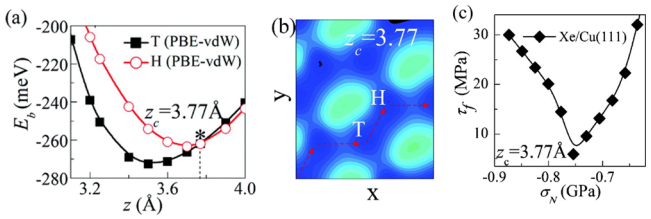


**Figure 17.** (a) Binding energy of Xe/Cu(111) using the PBE+vdW approach as a function of the RG−substrate distance $z$. The $E_b(z)$ curves undergo crossings at a critical distance (loads) $Z_c$ = 3.77 Å in the far-surface region. (b) Sliding potential energy landscape (meV) of a Xe monolayer over Cu(111) with an adatom-surface distance of $z_c$ = 3.77 Å. The dashed arrows present the actual path of sliding motion, where the PES feature can be changed by pressure. (c) Attraction-induced ultralow friction for Xe sliding over Cu(111) surface. Reproduced with permission from ref 169. Copyright 2017 The Royal Society of Chemistry.

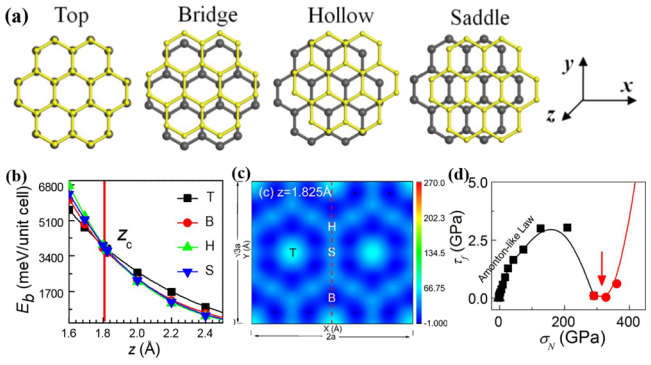


**Figure 18.** (a) High-symmetry top (T), bridge (B), hollow (H), and saddle (S) sites of the bilayer in a graphene/graphene sliding system. (b) Calculated binding energy $E_b(z)$ as a function of interplanar spacing ($z$) for graphene/graphene in the region of compression. The energy crossing occurring at critical distance $z_c$. (c) Pressure-driven flat PES corrugation for graphene/graphene at $z$ = 1.825 Å. (d) Frictional shear strength $\tau_f$ versus normal pressure $\sigma_N$. The black line refers to $\tau_f$ of corrugated PESs, while the red line refers to $\tau_f$ of countercorrugated PESs in the repulsive region. The red arrow is critical frictionless sliding in the high loading regime. Reproduced with permission from ref 170. Copyright 2018 ACS Publications.

be of considerable significance for technological applications.[169,170] Figure 17b shows the PES with a zero sliding energy barrier along the top-hollow path under the critical pressure at $Z_c$ = 3.77 Å for Xe/Cu(111). Furthermore, the attraction-induced collapse of friction ($\tau_f$) for the commensurate contact of Xe/Cu(111) in the low-load ($\sigma_N$) of the attractive regime in Figure 17c clearly shows the non-linear nature of the nanoscale friction at stretched separations. As the load decreases to the critical pressure (approximately −0.75 GPa), the friction force can be modulated to a theoretical zero value by decreasing the normal load to the critical value of $Z_c$ = 3.77 Å. Similar load-driven zero frictions were discovered for Xe/Pd(111) (at $\sigma_N$ = −2.2 GPa of $Z_c$ = 3.52 Å) and Ar/Cu(111) (at $\sigma_N$ = −0.83 GPa of $Z_c$ = 4.05 Å). These theoretical results provide useful guidelines for more studies of load-driven superlubricity for RG layers on metallic surfaces.

The tribological feature of substrates toward the motion of RG adsorbates can be tuned through surface modification, such as adding a graphene (GR) layer. We performed self-consistent vdW-DF calculations for the sliding friction of the Xe monolayer on the Au(111), graphene, and graphene-coated Au(111) substrates. Strikingly, the PESs of Xe/GR and Xe/GR/Au(111) are more corrugated than that of Xe/Au(111), indicating a low mobility of Xe on graphene. This gave insights into the understanding of counterintuitive experimental observations on worsened tribological properties after graphene coating. On the other hand, graphene/graphene sliding (cf. in Figure 18a) undergoes an abnormal transition from corrugated to essentially flattened PESs as depicted at a critical point of $Z_c$ = 1.825 Å, as shown in Figure 18b. Thus, the sliding friction decreases with increasing normal load and collapses to nearly zero under a critical pressure (see Figure 18c).[170] The lateral friction, $\tau_f$, increases with normal pressure for $\sigma_N$ < 160 GPa, showing the Amonton-like feature, as shown in Figure 18d. It then drops quickly and passes through a nearly zero value (red arrow) for $\sigma_N$ = 200−280 GPa before it increases again (red lines). This behavior was also found in other sliding systems, such as Xe/Cu, Pd/graphite, and $MoS_2$/$MoS_2$.

## 4. CONCLUSIONS

We reviewed the main features of different vdW approaches that are implemented in various DFT packages. Obviously, many theoretical studies of weak bonds are not included here. From examples discussed above, one may see that the development of numerous vdW functionals in the past decade has already made a significant impact on theoretical studies of physisorption systems toward the chemical accuracy that is required for making reliable theoretical predictions of diverse properties from catalysis and tribology to new areas such as functional 2D materials. Nevertheless, the consistency among vdW approaches is still a serious issue in this realm.

It is plausible that the simple DFT-$D_n$ correction methods can efficiently provide reasonably good vdW forces in various adsorption and catalytic processes on metal surfaces, and the transferability of the $C_6$ coefficients is also continuously improved. In vdW-DF methods, the choice of different exchange functionals and the nonlocal correlation forms still causes noticeable discrepancies. Both revPBE (in vdW-DF1) and rPW86 (in vdW-DF2) exchanges underestimate dispersion forces between molecules and substrates. While the dispersion correction (DFT-D3, DFT-TS, etc.) and optimized non-local correlation methods (optPBE-vdW, optB88-vdW, and optB86b-vdW) can improve the adsorption energies of molecules, their accuracy for the determination of reaction barriers is yet to be examined. Additionally, the many-body effects may result in very long-range quantum fluctuation on the metal surface, labeled as the type-C dispersion interaction by Dobson,[171] which has not been treated in the current vdW functionals. More efforts are required to overcome these problems and to establish more universal and efficient vdW-inclusive DFT methods for massive studies of physical or chemical processes in which the dispersion forces are curial.

While the London dispersion was discussed in textbooks as the origin of vdW forces, most DFT calculations indicated that the inclusion of vdW functional leads to noticeable charge redistribution and hence the contributions from permanent dipoles or additional charge rearrangements are also important, as mentioned by Feynman decades ago.[172] It is conceivable that the dispersion forces are also involved in most chemical bonds (ionic or covalent), but their effect on the charge distribution becomes noticeable only when strong forces disappear or are sufficiently reduced. We perceive that the vdW bonds appear more like "weak-covalent" bonds and can be


https://dx.doi.org/10.1021/acs.jpcc.0c02293
J. Phys. Chem. C 2020, 124, 16926−16942

traced by charge accumulation, as evidenced in our recent work on several systems.[8,9] This provides a bridge to connect DFT charge maps and PESs to itProbe images for studies of weak bonds in molecular systems, which may open new research areas in the future. For example, quantitative experimental and theoretical studies of hydrogen bonding in biomolecules with real space images may solve challenging issues in life science. It is foreseeable that DFT studies with a more accurate and universal version of the vdW functional will become exceedingly powerful in many research areas.

## ■ ASSOCIATED CONTENT

### Special Issue Paper

This paper was intended for the Toward Chemistry in Real Space and Real Time Virtual Special Issue, published May 14, 2020.

## ■ AUTHOR INFORMATION


### Corresponding Author

**Ruqian Wu** − *Department of Physics and Astronomy, University of California, Irvine, California 92697-4575, United States;* orcid.org/0000-0002-6156-7874; Email: wur@uci.edu

### Authors

**Dingwang Yuan** − *College of Materials Science and Engineering, State Key Laboratory of Chemo/Biosensing and Chemometrics, Hunan University, Changsha 410082, China*

**Yanning Zhang** − *Institute of Fundamental and Frontier Sciences, University of Electronic Science and Technology of China, Chengdu 611731, China;* orcid.org/0000-0002-3839-2965

**Wilson Ho** − *Department of Physics and Astronomy and Department of Chemistry, University of California, Irvine, California 92697-4575, United States;* orcid.org/0000-0003-3884-2142

Complete contact information is available at: https://pubs.acs.org/10.1021/acs.jpcc.0c02293


### Author Contributions

△D.Y. and Y.Z. contributed equally to this work.

### Notes

The authors declare no competing financial interest.

## ■ ACKNOWLEDGMENTS

This work is supported by the National Science Foundation under grant no. CHE-1905121 and the Center for Chemical Innovation on Chemistry at the Space-Time Limit (CaSTL) under grant no. CHE-0802913. D.W.Y. acknowledges support by the National Natural Science Foundation of China (grant no. 11674091). Y.N.Z. acknowledges support by the National Natural Science Foundation of China (grant no. 11874005).

## ■ REFERENCES


(1) Siler, C. G. F.; Madix, R. J.; Friend, C. M. Designing for Selectivity: Weak Interactions and the Competition for Reactive Sites on Gold Catalysts. *Faraday Discuss.* **2016**, *188*, 355−368.

(2) Rodriguez-Reyes, J. C. F.; Siler, C. G. F.; Liu, W.; Tkatchenko, A.; Friend, C. M.; Madix, R. J. Van Der Waals Interactions Determine Selectivity in Catalysis by Metallic Gold. *J. Am. Chem. Soc.* **2014**, *136*, 13333−13340.

(3) Schnur, S.; Groß, A. Challenges in the First-Principles Description of Reactions in Electrocatalysis. *Catal. Today* **2011**, *165*, 129−137.

(4) López, N.; Almora-Barrios, N.; Carchini, G.; Błoński, P.; Bellarosa, L.; García-Muelas, R.; Novell-Leruth, G.; García-Mota, M. State-of-the-Art and Challenges in Theoretical Simulations of Heterogeneous Catalysis at the Microscopic Level. *Catal. Sci. Technol.* **2012**, *2*, 2405.

(5) Prats, H.; Gamallo, P.; Sayós, R.; Illas, F. Unexpectedly Large Impact of van Der Waals Interactions on the Description of Heterogeneously Catalyzed Reactions: The Water Gas Shift Reaction on Cu(321) as a Case Example. *Phys. Chem. Chem. Phys.* **2016**, *18*, 2792−2801.

(6) Liu, W.; Tkatchenko, A.; Scheffler, M. Modeling Adsorption and Reactions of Organic Molecules at Metal Surfaces. *Acc. Chem. Res.* **2014**, *47*, 3369−3377.

(7) Zhang, S.; Ma, T.; Erdemir, A.; Li, Q. Tribology of Two-Dimensional Materials: From Mechanisms to Modulating Strategies. *Mater. Today* **2019**, *26*, 67−86.

(8) Han, Z.; Czap, G.; Chiang, C.-I.; Xu, C.; Wagner, P. J.; Wei, X.; Zhang, Y.; Wu, R.; Ho, W. Imaging the Halogen Bond in Self-Assembled Halogenbenzenes on Silver. *Science* **2017**, *358*, 206−210.

(9) Han, Z.; Wei, X.; Xu, C.; Chiang, C.-I.; Zhang, Y.; Wu, R.; Ho, W. Imaging van Der Waals Interactions. *J. Phys. Chem. Lett.* **2016**, *7*, 5205−5211.

(10) Chiang, C.-I.; Xu, C.; Han, Z.; Ho, W. Real-Space Imaging of Molecular Structure and Chemical Bonding by Single-Molecule Inelastic Tunneling Probe. *Science* **2014**, *344*, 885−888.

(11) Su, G.; Yang, S.; Jiang, Y.; Li, J.; Li, S.; Ren, J.-C.; Liu, W. Modeling Chemical Reactions on Surfaces: The Roles of Chemical Bonding and van Der Waals Interactions. *Prog. Surf. Sci.* **2019**, *94*, 100561.

(12) Campbell, C. T. Energies of Adsorbed Catalytic Intermediates on Transition Metal Surfaces: Calorimetric Measurements and Benchmarks for Theory. *Acc. Chem. Res.* **2019**, *52*, 984−993.

(13) Weymouth, A. J.; Hofmann, T.; Giessibl, F. J. Quantifying Molecular Stiffness and Interaction with Lateral Force Microscopy. *Science* **2014**, *343*, 1120−1122.

(14) Liu, W.; Maaß, F.; Willenbockel, M.; Bronner, C.; Schulze, M.; Soubatch, S.; Tautz, F. S.; Tegeder, P.; Tkatchenko, A. Quantitative Prediction of Molecular Adsorption: Structure and Binding of Benzene on Coinage Metals. *Phys. Rev. Lett.* **2015**, *115*, No. 036104.

(15) Carey, S. J.; Zhao, W.; Campbell, C. T. Energetics of Adsorbed Benzene on Ni(111) and Pt(111) by Calorimetry. *Surf. Sci.* **2018**, *676*, 9−16.

(16) Campbell, C. T.; Sellers, J. R. V. Enthalpies and Entropies of Adsorption on Well-Defined Oxide Surfaces: Experimental Measurements. *Chem. Rev.* **2013**, *113*, 4106−4135.

(17) Zhao, W.; Carey, S. J.; Morgan, S. E.; Campbell, C. T. Energetics of Adsorbed Formate and Formic Acid on Ni(111) by Calorimetry. *J. Catal.* **2017**, *352*, 300−304.

(18) Silbaugh, T. L.; Campbell, C. T. Energies of Formation Reactions Measured for Adsorbates on Late Transition Metal Surfaces. *J. Phys. Chem. C* **2016**, *120*, 25161−25172.

(19) Silbaugh, T. L.; Karp, E. M.; Campbell, C. T. Energetics of Formic Acid Conversion to Adsorbed Formates on Pt(111) by Transient Calorimetry. *J. Am. Chem. Soc.* **2014**, *136*, 3964−3971.

(20) Bligaard, T.; Bullock, R. M.; Campbell, C. T.; Chen, J. G.; Gates, B. C.; Gorte, R. J.; Jones, C. W.; Jones, W. D.; Kitchin, J. R.; Scott, S. L. Toward Benchmarking in Catalysis Science: Best Practices, Challenges, and Opportunities. *ACS Catal.* **2016**, *6*, 2590−2602.

(21) Shiozawa, Y.; Koitaya, T.; Mukai, K.; Yoshimoto, S.; Yoshinobu, J. Quantitative Analysis of Desorption and Decomposition Kinetics of Formic Acid on Cu(111): The Importance of Hydrogen Bonding between Adsorbed Species. *J. Chem. Phys.* **2015**, *143*, 234707.

(22) Yuan, D.; Han, Z.; Czap, G.; Chiang, C.-I.; Xu, C.; Ho, W.; Wu, R. Quantitative Understanding of van Der Waals Interactions by Analyzing the Adsorption Structure and Low-Frequency Vibrational Modes of Single Benzene Molecules on Silver. *J. Phys. Chem. Lett.* **2016**, *7*, 2228−2233.

(23) Krim, J. Friction and Energy Dissipation Mechanisms in Adsorbed Molecules and Molecularly Thin Films. *Adv. Phys.* **2012**, *61*, 155−323.
(24) Bruch, L. W.; Diehl, R. D.; Venables, J. A. Progress in the Measurement and Modeling of Physisorbed Layers. *Rev. Mod. Phys.* **2007**, *79*, 1381−1454.
(25) Weymouth, A. J.; Meuer, D.; Mutombo, P.; Wutscher, T.; Ondracek, M.; Jelinek, P.; Giessibl, F. J. Atomic Structure Affects the Directional Dependence of Friction. *Phys. Rev. Lett.* **2013**, *111*, 126103.
(26) Bruschi, L.; Pierno, M.; Fois, G.; Ancilotto, F.; Mistura, G.; Boragno, C.; Buatier de Mongeot, F.; Valbusa, U. Friction Reduction of Ne Monolayers on Preplated Metal Surfaces. *Phys. Rev. B* **2010**, *81*, 115419.
(27) Bruschi, L.; Fois, G.; Pontarollo, A.; Mistura, G.; Torre, B.; Buatier de Mongeot, F.; Boragno, C.; Buzio, R.; Valbusa, U. Structural Depinning of Ne Monolayers on Pb at T < 6.5 K. *Phys. Rev. Lett.* **2006**, *96*, 216101.
(28) Caragiu, M.; Seyller, T.; Diehl, R. D. Dynamical LEED Study of Pd ( 111 ) − ( 3 × 3 ) R 30 ° -Xe. *Phys. Rev. B* **2002**, *66*, 195411.
(29) Herbig, C.; Åhlgren, E. H.; Schröder, U. A.; Martínez-Galera, A. J.; Arman, M. A.; Kotakoski, J.; Knudsen, J.; Krasheninnikov, A. V.; Michely, T. Xe Irradiation of Graphene on Ir(111): From Trapping to Blistering. *Phys. Rev. B* **2015**, *92*, No. 085429.
(30) Bendounan, A. Adsorption Properties of Xe on Ag/Cu(111) System: Real-Time Photoemission Investigation. *J. Phys. Chem. C* **2016**, *120*, 24279−24286.
(31) Krim, J.; Solina, D. H.; Chiarello, R. Nanotribology of a Kr Monolayer: A Quartz-Crystal Microbalance Study of Atomic-Scale Friction. *Phys. Rev. Lett.* **1991**, *66*, 181−184.
(32) Pierno, M.; Bruschi, L.; Fois, G.; Mistura, G.; Boragno, C.; de Mongeot, F. B.; Valbusa, U. Nanofriction of Neon Films on Superconducting Lead. *Phys. Rev. Lett.* **2010**, *105*, No. 016102.
(33) Stöhr, M.; Van Voorhis, T.; Tkatchenko, A. Theory and Practice of Modeling van Der Waals Interactions in Electronic-Structure Calculations. *Chem. Soc. Rev.* **2019**, *48*, 4118−4154.
(34) Klimeš, J.; Bowler, D. R.; Michaelides, A. Van Der Waals Density Functionals Applied to Solids. *Phys. Rev. B* **2011**, *83*, 195131.
(35) Ding, Z.; Liu, W.; Li, S.; Zhang, D.; Zhao, Y.; Lavernia, E. J.; Zhu, Y. Contribution of van Der Waals Forces to the Plasticity of Magnesium. *Acta Mater.* **2016**, *107*, 127−132.
(36) Liu, W.; Ruiz, V. G.; Zhang, G.-X.; Santra, B.; Ren, X.; Scheffler, M.; Tkatchenko, A. Structure and Energetics of Benzene Adsorbed on Transition-Metal Surfaces: Density-Functional Theory with van Der Waals Interactions Including Collective Substrate Response. *New J. Phys.* **2013**, *15*, No. 053046.
(37) Zhang, G.-X.; Reilly, A. M.; Tkatchenko, A.; Scheffler, M. Performance of Various Density-Functional Approximations for Cohesive Properties of 64 Bulk Solids. *New J. Phys.* **2018**, *20*, No. 063020.
(38) Tran, F.; Kalantari, L.; Traoré, B.; Rocquefelte, X.; Blaha, P. Nonlocal van Der Waals Functionals for Solids: Choosing an Appropriate One. *Phys. Rev. Mater.* **2019**, *3*, No. 063602.
(39) Patra, A.; Bates, J. E.; Sun, J.; Perdew, J. P. Properties of Real Metallic Surfaces: Effects of Density Functional Semilocality and van Der Waals Nonlocality. *Proc. Natl. Acad. Sci. U. S. A.* **2017**, *114*, E9188−E9196.
(40) Kim, M.; Kim, W. J.; Lee, E. K.; Lebègue, S.; Kim, H. Recent Development of Atom-Pairwise van Der Waals Corrections for Density Functional Theory: From Molecules to Solids. *Int. J. Quantum Chem.* **2016**, *116*, 598−607.
(41) Langreth, D. C.; Dion, M.; Rydberg, H.; Schröder, E.; Hyldgaard, P.; Lundqvist, B. I. Van Der Waals Density Functional Theory with Applications. *Int. J. Quantum Chem.* **2005**, *101*, 599−610.
(42) Hermann, J.; DiStasio, R. A., Jr.; Tkatchenko, A. First-Principles Models for van Der Waals Interactions in Molecules and Materials: Concepts, Theory, and Applications. *Chem. Rev.* **2017**, *117*, 4714−4758.
(43) Klimeš, J.; Michaelides, A. Perspective: Advances and Challenges in Treating van Der Waals Dispersion Forces in Density Functional Theory. *J. Chem. Phys.* **2012**, *137*, 120901.
(44) Grimme, S. Accurate Description of van Der Waals Complexes by Density Functional Theory Including Empirical Corrections. *J. Comput. Chem.* **2004**, *25*, 1463−1473.
(45) Grimme, S. Semiempirical GGA-Type Density Functional Constructed with a Long-Range Dispersion Correction. *J. Comput. Chem.* **2006**, *27*, 1787−1799.
(46) Grimme, S.; Antony, J.; Ehrlich, S.; Krieg, H. A Consistent and Accurate Ab Initio Parametrization of Density Functional Dispersion Correction (DFT-D) for the 94 Elements H-Pu. *J. Chem. Phys.* **2010**, *132*, 154104.
(47) Grimme, S.; Ehrlich, S.; Goerigk, L. Effect of the Damping Function in Dispersion Corrected Density Functional Theory. *J. Comput. Chem.* **2011**, *32*, 1456−1465.
(48) Tkatchenko, A.; Scheffler, M. Accurate Molecular Van Der Waals Interactions from Ground-State Electron Density and Free-Atom Reference Data. *Phys. Rev. Lett.* **2009**, *102*, No. 073005.
(49) Tkatchenko, A.; DiStasio, R. A.; Car, R.; Scheffler, M. Accurate and Efficient Method for Many-Body van Der Waals Interactions. *Phys. Rev. Lett.* **2012**, *108*, 236402.
(50) Bučko, T.; Lebègue, S.; Ángyán, J. G.; Hafner, J. Extending the Applicability of the Tkatchenko-Scheffler Dispersion Correction via Iterative Hirshfeld Partitioning. *J. Chem. Phys.* **2014**, *141*, No. 034114.
(51) Bučko, T.; Lebègue, S.; Hafner, J.; Ángyán, J. G. Improved Density Dependent Correction for the Description of London Dispersion Forces. *J. Chem. Theory Comput.* **2013**, *9*, 4293−4299.
(52) Steinmann, S. N.; Corminboeuf, C. Comprehensive Benchmarking of a Density-Dependent Dispersion Correction. *J. Chem. Theory Comput.* **2011**, *7*, 3567−3577.
(53) Steinmann, S. N.; Corminboeuf, C. A Generalized-Gradient Approximation Exchange Hole Model for Dispersion Coefficients. *J. Chem. Phys.* **2011**, *134*, No. 044117.
(54) Caldeweyher, E.; Ehlert, S.; Hansen, A.; Neugebauer, H.; Spicher, S.; Bannwarth, C.; Grimme, S. A Generally Applicable Atomic-Charge Dependent London Dispersion Correction. *J. Chem. Phys.* **2019**, *150*, 154122.
(55) Caldeweyher, E.; Mewes, J.-M.; Ehlert, S.; Grimme, S. Extension and Evaluation of the D4 London Dispersion Model for Periodic Systems. *Phys. Chem. Chem. Phys.* **2020**, *22*, 8499−8512.
(56) Johnson, E. R.; Becke, A. D. A Post-Hartree−Fock Model of Intermolecular Interactions. *J. Chem. Phys.* **2005**, *123*, No. 024101.
(57) Ambrosetti, A.; Reilly, A. M.; DiStasio, R. A., Jr.; Tkatchenko, A. Long-Range Correlation Energy Calculated from Coupled Atomic Response Functions. *J. Chem. Phys.* **2014**, *140*, 18A508.
(58) DiStasio, R. A., Jr.; Gobre, V. V.; Tkatchenko, A. Many-Body van Der Waals Interactions in Molecules and Condensed Matter. *J. Phys.: Condens. Matter* **2014**, *26*, 213202.
(59) Bučko, T.; Lebègue, S.; Gould, T.; Ángyán, J. G. Many-Body Dispersion Corrections for Periodic Systems: An Efficient Reciprocal Space Implementation. *J. Phys.: Condens. Matter* **2016**, *28*, No. 045201.
(60) Dion, M.; Rydberg, H.; Schröder, E.; Langreth, D. C.; Lundqvist, B. I. Van Der Waals Density Functional for General Geometries. *Phys. Rev. Lett.* **2004**, *92*, 246401.
(61) Lee, K.; Murray, É. D.; Kong, L.; Lundqvist, B. I.; Langreth, D. C. Higher-Accuracy van Der Waals Density Functional. *Phys. Rev. B* **2010**, *82*, No. 081101.
(62) Murray, É. D.; Lee, K.; Langreth, D. C. Investigation of Exchange Energy Density Functional Accuracy for Interacting Molecules. *J. Chem. Theory Comput.* **2009**, *5*, 2754−2762.
(63) Yuan, D.; Liao, H.; Hu, W. Assessment of van Der Waals Inclusive Density Functional Theory Methods for Adsorption and Selective Dehydrogenation of Formic Acid on Pt(111) Surface. *Phys. Chem. Chem. Phys.* **2019**, *21*, 21049−21056.
(64) Freire, R. L. H.; Guedes-Sobrinho, D.; Kiejna, A.; Da Silva, J. L. F. Comparison of the Performance of van Der Waals Dispersion


https://dx.doi.org/10.1021/acs.jpcc.0c02293
J. Phys. Chem. C 2020, 124, 16926−16942

Functionals in the Description of Water and Ethanol on Transition Metal Surfaces. *J. Phys. Chem. C* **2018**, *122*, 1577−1588.
(65) Klimeš, J.; Bowler, D. R.; Michaelides, A. Chemical Accuracy for the van Der Waals Density Functional. *J. Phys.: Condens. Matter* **2010**, *22*, No. 022201.
(66) Berland, K.; Hyldgaard, P. Exchange Functional That Tests the Robustness of the Plasmon Description of the van Der Waals Density Functional. *Phys. Rev. B* **2014**, *89*, No. 035412.
(67) Cooper, V. R. Van Der Waals Density Functional: An Appropriate Exchange Functional. *Phys. Rev. B* **2010**, *81*, 161104.
(68) Jiao, Y.; Schröder, E.; Hyldgaard, P. Extent of Fock-Exchange Mixing for a Hybrid van Der Waals Density Functional? *J. Chem. Phys.* **2018**, *148*, 194115.
(69) Berland, K.; Jiao, Y.; Lee, J.-H.; Rangel, T.; Neaton, J. B.; Hyldgaard, P. Assessment of Two Hybrid van Der Waals Density Functionals for Covalent and Non-Covalent Binding of Molecules. *J. Chem. Phys.* **2017**, *146*, 234106.
(70) Vydrov, O. A.; Van Voorhis, T. Nonlocal van Der Waals Density Functional Made Simple. *Phys. Rev. Lett.* **2009**, *103*, No. 063004.
(71) Vydrov, O. A.; Van Voorhis, T. Improving the Accuracy of the Nonlocal van Der Waals Density Functional with Minimal Empiricism. *J. Chem. Phys.* **2009**, *130*, 104105.
(72) Vydrov, O. A.; Van Voorhis, T. Nonlocal van Der Waals Density Functional: The Simpler the Better. *J. Chem. Phys.* **2010**, *133*, 244103.
(73) Sabatini, R.; Gorni, T.; de Gironcoli, S. Nonlocal van Der Waals Density Functional Made Simple and Efficient. *Phys. Rev. B* **2013**, *87*, No. 041108.
(74) Peng, H.; Yang, Z.-H.; Perdew, J. P.; Sun, J. Versatile van Der Waals Density Functional Based on a Meta-Generalized Gradient Approximation. *Phys. Rev. X* **2016**, *6*, No. 041005.
(75) Patra, A.; Jana, S.; Samal, P. Performance of Tao−Mo Semilocal Functional with RVV10 Dispersion-Correction: Influence of Different Correlation. *J. Phys. Chem. A* **2019**, *123*, 10582−10593.
(76) Adhikari, S.; Tang, H.; Neupane, B.; Ruzsinszky, A.; Csonka, G. I. Molecule-Surface Interaction from van Der Waals-Corrected Semilocal Density Functionals: The Example of Thiophene on Transition-Metal Surfaces. *Phys. Rev. Mater.* **2020**, *4*, No. 025005.
(77) Hermann, J.; Tkatchenko, A. Density-Functional Model for van Der Waals Interactions: Unifying Many-Body Atomic Approaches with Nonlocal Functionals. *Phys. Rev. Lett.* **2020**, *124*, 146401.
(78) Vydrov, O. A.; Van Voorhis, T. Dispersion Interactions from a Local Polarizability Model. *Phys. Rev. A* **2010**, *81*, No. 062708.
(79) Tkatchenko, A.; Ambrosetti, A.; DiStasio, R. A., Jr. Interatomic Methods for the Dispersion Energy Derived from the Adiabatic Connection Fluctuation-Dissipation Theorem. *J. Chem. Phys.* **2013**, *138*, No. 074106.
(80) Lu, D.; Li, Y.; Rocca, D.; Galli, G. *Ab Initio* Calculation of van Der Waals Bonded Molecular Crystals. *Phys. Rev. Lett.* **2009**, *102*, 206411.
(81) Yang, J.; Hu, W.; Usvyat, D.; Matthews, D.; Schütz, M.; Chan, G. K.-L. Ab Initio Determination of the Crystalline Benzene Lattice Energy to Sub-Kilojoule/Mole Accuracy. *Science* **2014**, *345*, 640.
(82) Azadi, S.; Kühne, T. D. Quantum Monte Carlo Calculations of van Der Waals Interactions between Aromatic Benzene Rings. *Phys. Rev. B* **2018**, *97*, 205428.
(83) Harl, J.; Schimka, L.; Kresse, G. Assessing the Quality of the Random Phase Approximation for Lattice Constants and Atomization Energies of Solids. *Phys. Rev. B* **2010**, *81*, 115126.
(84) Garrido Torres, J. A.; Ramberger, B.; Früchtl, H. A.; Schaub, R.; Kresse, G. Adsorption Energies of Benzene on Close Packed Transition Metal Surfaces Using the Random Phase Approximation. *Phys. Rev. Mater.* **2017**, *1*, No. 060803.
(85) Snyder, J. C.; Rupp, M.; Hansen, K.; Müller, K.-R.; Burke, K. Finding Density Functionals with Machine Learning. *Phys. Rev. Lett.* **2012**, *108*, 253002.
(86) Li, L.; Snyder, J. C.; Pelaschier, I. M.; Huang, J.; Niranjan, U.-N.; Duncan, P.; Rupp, M.; Müller, K.-R.; Burke, K. Understanding Machine-Learned Density Functionals. *Int. J. Quantum Chem.* **2016**, *116*, 819−833.
(87) Hollingsworth, J.; Li, L.; Baker, T. E.; Burke, K. Can Exact Conditions Improve Machine-Learned Density Functionals? *J. Chem. Phys.* **2018**, *148*, 241743.
(88) Seino, J.; Kageyama, R.; Fujinami, M.; Ikabata, Y.; Nakai, H. Semi-Local Machine-Learned Kinetic Energy Density Functional with Third-Order Gradients of Electron Density. *J. Chem. Phys.* **2018**, *148*, 241705.
(89) Liu, Q.; Wang, J.; Du, P.; Hu, L.; Zheng, X.; Chen, G. Improving the Performance of Long-Range-Corrected Exchange-Correlation Functional with an Embedded Neural Network. *J. Phys. Chem. A* **2017**, *121*, 7273−7281.
(90) Mezei, P. D.; von Lilienfeld, O. A. Non-Covalent Quantum Machine Learning Corrections to Density Functionals. *J. Chem. Theory Comput.* **2020**, *16*, 2647−2653.
(91) Moreno, J. R.; Carleo, G.; Georges, A. *Deep Learning the Hohenberg-Kohn Maps of Density Functional Theory*. 2019 arXiv:1911.03580 *[cond-mat, physics:quant-ph]*. https://arxiv.org/abs/1911.03580.
(92) Dick, S.; Fernandez-Serra, M. Machine Learning Accurate Exchange and Correlation Functionals of the Electronic Density. 2019, DOI: 10.26434/chemrxiv.9947312.v2.
(93) Lundgaard, K. T.; Wellendorff, J.; Voss, J.; Jacobsen, K. W.; Bligaard, T. MBEEF-VdW: Robust Fitting of Error Estimation Density Functionals. *Phys. Rev. B* **2016**, *93*, 235162.
(94) Wellendorff, J.; Lundgaard, K. T.; Møgelhøj, A.; Petzold, V.; Landis, D. D.; Nørskov, J. K.; Bligaard, T.; Jacobsen, K. W. Density Functionals for Surface Science: Exchange-Correlation Model Development with Bayesian Error Estimation. *Phys. Rev. B* **2012**, *85*, 235149.
(95) Wellendorff, J.; Lundgaard, K. T.; Jacobsen, K. W.; Bligaard, T. MBEEF: An Accurate Semi-Local Bayesian Error Estimation Density Functional. *J. Chem. Phys.* **2014**, *140*, 144107.
(96) Proppe, J.; Gugler, S.; Reiher, M. Gaussian Process-Based Refinement of Dispersion Corrections. *J. Chem. Theory Comput.* **2019**, *15*, 6046−6060.
(97) Veit, M.; Jain, S. K.; Bonakala, S.; Rudra, I.; Hohl, D.; Csányi, G. Equation of State of Fluid Methane from First Principles with Machine Learning Potentials. *J. Chem. Theory Comput.* **2019**, *15*, 2574−2586.
(98) Wellendorff, J.; Silbaugh, T. L.; Garcia-Pintos, D.; Nørskov, J. K.; Bligaard, T.; Studt, F.; Campbell, C. T. A Benchmark Database for Adsorption Bond Energies to Transition Metal Surfaces and Comparison to Selected DFT Functionals. *Surf. Sci.* **2015**, *640*, 36−44.
(99) Luo, Q.; Feng, G.; Beller, M.; Jiao, H. Formic Acid Dehydrogenation on Ni(111) and Comparison with Pd(111) and Pt(111). *J. Phys. Chem. C* **2012**, *116*, 4149−4156.
(100) Hammer, B.; Hansen, L. B.; Nørskov, J. K. Improved Adsorption Energetics within Density-Functional Theory Using Revised Perdew-Burke-Ernzerhof Functionals. *Phys. Rev. B* **1999**, *59*, 7413−7421.
(101) Gautier, S.; Steinmann, S. N.; Michel, C.; Fleurat-Lessard, P.; Sautet, P. Molecular Adsorption at Pt(111). How Accurate Are DFT Functionals? *Phys. Chem. Chem. Phys.* **2015**, *17*, 28921−28930.
(102) Jia, X.; An, W. Adsorption of Monocyclic Aromatics on Transition Metal Surfaces: Insight into Variation of Binding Strength from First-Principles. *J. Phys. Chem. C* **2018**, 21897−21909.
(103) Chwee, T. S.; Sullivan, M. B. Adsorption Studies of $C_6H_6$on Cu (111), Ag (111), and Au (111) within Dispersion Corrected Density Functional Theory. *J. Chem. Phys.* **2012**, *137*, 134703.
(104) Matos, J.; Yildirim, H.; Kara, A. Insight into the Effect of Long Range Interactions for the Adsorption of Benzene on Transition Metal (110) Surfaces. *J. Phys. Chem. C* **2015**, *119*, 1886−1897.
(105) Liu, W.; Carrasco, J.; Santra, B.; Michaelides, A.; Scheffler, M.; Tkatchenko, A. Benzene Adsorbed on Metals: Concerted Effect of Covalency and van Der Waals Bonding. *Phys. Rev. B* **2012**, *86*, 245405.

(106) Yildirim, H.; Greber, T.; Kara, A. Trends in Adsorption Characteristics of Benzene on Transition Metal Surfaces: Role of Surface Chemistry and van Der Waals Interactions. *J. Phys. Chem. C* **2013**, *117*, 20572−20583.
(107) Hensley, A. J. R.; Ghale, K.; Rieg, C.; Dang, T.; Anderst, E.; Studt, F.; Campbell, C. T.; McEwen, J. S.; Xu, Y. DFT-Based Method for More Accurate Adsorption Energies: An Adaptive Sum of Energies from RPBE and VdW Density Functionals. *J. Phys. Chem. C* **2017**, *121*, 4937−4945.
(108) Muttaqien, F.; Hamamoto, Y.; Hamada, I.; Inagaki, K.; Shiozawa, Y.; Mukai, K.; Koitaya, T.; Yoshimoto, S.; Yoshinobu, J.; Morikawa, Y. $CO_2$ Adsorption on the Copper Surfaces: Van Der Waals Density Functional and TPD Studies. *J. Chem. Phys.* **2017**, *147*, No. 094702.
(109) Hamada, I. Van Der Waals Density Functional Made Accurate. *Phys. Rev. B* **2014**, *89*, 121103.
(110) Chen, W.; Cubuk, E. D.; Montemore, M. M.; Reece, C.; Madix, R. J.; Friend, C. M.; Kaxiras, E. A Comparative Ab Initio Study of Anhydrous Dehydrogenation of Linear-Chain Alcohols on Cu(110). *J. Phys. Chem. C* **2018**, *122*, 7806−7815.
(111) Cheenicode Kabeer, F.; Chen, W.; Madix, R. J.; Friend, C. M.; Tkatchenko, A. First-Principles Study of Alkoxides Adsorbed on Au(111) and Au(110) Surfaces: Assessing the Roles of Noncovalent Interactions and Molecular Structures in Catalysis. *J. Phys. Chem. C* **2017**, *121*, 27905−27914.
(112) Xu, Y.; Chen, W.; Kaxiras, E.; Friend, C. M.; Madix, R. J. General Effect of van Der Waals Interactions on the Stability of Alkoxy Intermediates on Metal Surfaces. *J. Phys. Chem. B* **2018**, *122*, 555−560.
(113) Janthon, P.; Viñes, F.; Sirijaraensre, J.; Limtrakul, J.; Illas, F. Adding Pieces to the CO/Pt(111) Puzzle: The Role of Dispersion. *J. Phys. Chem. C* **2017**, *121*, 3970−3977.
(114) Nørskov, J. K.; Studt, F.; Abild-Pedersen, F.; Bligaard, T. *Fundamental concepts in heterogeneous catalysis*, Wiley, Hoboken, New Jersey, 2014.
(115) Quan, J.; Muttaqien, F.; Kondo, T.; Kozarashi, T.; Mogi, T.; Imabayashi, T.; Hamamoto, Y.; Inagaki, K.; Hamada, I.; Morikawa, Y.; et al. Vibration-Driven Reaction of $CO_2$ on Cu Surfaces via Eley−Rideal-Type Mechanism. *Nat. Chem.* **2019**, *11*, 722−729.
(116) Shirhatti, P. R.; Rahinov, I.; Golibrzuch, K.; Werdecker, J.; Geweke, J.; Altschäffel, J.; Kumar, S.; Auerbach, D. J.; Bartels, C.; Wodtke, A. M. Observation of the Adsorption and Desorption of Vibrationally Excited Molecules on a Metal Surface. *Nature Chem* **2018**, *10*, 592−598.
(117) Wang, H.; Li, S.; He, H.; Yu, A.; Toledo, F.; Han, Z.; Ho, W.; Wu, R. Trapping and Characterization of a Single Hydrogen Molecule in a Continuously Tunable Nanocavity. *J. Phys. Chem. Lett.* **2015**, *6*, 3453−3457.
(118) Garrido Torres, J. A.; Finley, K. L.; Früchtl, H. A.; Webb, P. B.; Schaub, R. Strong Substrate Mediation of Attractive Lateral Interactions of CO on Cu(110). *Langmuir* **2019**, *35*, 608−614.
(119) Shiotari, A.; Odani, T.; Sugimoto, Y. Torque-Induced Change in Configuration of a Single NO Molecule on Cu(110). *Phys. Rev. Lett.* **2018**, *121*, 116101.
(120) Han, Z.; Czap, G.; Xu, C.; Chiang, C.; Yuan, D.; Wu, R.; Ho, W. Probing Intermolecular Coupled Vibrations between Two Molecules. *Phys. Rev. Lett.* **2017**, *118*, No. 036801.
(121) Ihm, Y.; Park, C.; Jakowski, J.; Morris, J. R.; Shim, J. H.; Kim, Y.-H.; Sumpter, B. G.; Yoon, M. Assessing the Predictive Power of Density Functional Theory in Finite-Temperature Hydrogen Adsorption/Desorption Thermodynamics. *J. Phys. Chem. C* **2018**, *122*, 26189−26195.
(122) Karakalos, S.; Xu, Y.; Cheenicode Kabeer, F.; Chen, W.; Rodríguez-Reyes, J. C. F.; Tkatchenko, A.; Kaxiras, E.; Madix, R. J.; Friend, C. M. Noncovalent Bonding Controls Selectivity in Heterogeneous Catalysis: Coupling Reactions on Gold. *J. Am. Chem. Soc.* **2016**, *138*, 15243−15250.
(123) Goldsmith, B. R.; Florian, J.; Liu, J.-X.; Gruene, P.; Lyon, J. T.; Rayner, D. M.; Fielicke, A.; Scheffler, M.; Ghiringhelli, L. M. Two-to-Three Dimensional Transition in Neutral Gold Clusters: The Crucial Role of van Der Waals Interactions and Temperature. *Phys. Rev. Mater.* **2019**, *3*, No. 016002.
(124) Avelar, J.; Bruix, A.; Garza, J.; Vargas, R. Van Der Waals Exchange-Correlation Functionals over Bulk and Surface Properties of Transition Metals. *J. Phys.: Condens. Matter* **2019**, *31*, 315501.
(125) Nair, A. S.; Pathak, B. *Importance of Dispersion and Relativistic Effects for ORR Overpotential Calculation on Pt(111) Surface*. 2019 arXiv:1908.08697v1[cond-mat.mtrl-sci]. https://arxiv.org/abs/1908.08697.
(126) Pham, T. L. M.; Vo, D.-V. N.; Nguyen, H. N. T.; Pham-Tran, N.-N. C-H versus O-H Bond Scission in Methanol Decomposition on Pt(111): Role of the Dispersion Interaction. *Appl. Surf. Sci.* **2019**, *481*, 1327−1334.
(127) Mallikarjun Sharada, S.; Bligaard, T.; Luntz, A. C.; Kroes, G.-J.; Nørskov, J. K. SBH10: A Benchmark Database of Barrier Heights on Transition Metal Surfaces. *J. Phys. Chem. C* **2017**, *121*, 19807−19815.
(128) Wijzenbroek, M.; Kroes, G. J. The Effect of the Exchange-Correlation Functional on $H_2$ Dissociation on Ru(0001). *J. Chem. Phys.* **2014**, *140*, No. 084702.
(129) Maiyalagan, T., Saji, V. S., Eds. *Electrocatalysts for Low Temperature Fuel Cells: Funda- mentals and Recent Trends*; Wiley-VCH Verlag GmbH & Co. KGaA: Weinheim, Germany, 2017.
(130) Yu, W.-Y.; Mullen, G. M.; Flaherty, D. W.; Mullins, C. B. Selective Hydrogen Production from Formic Acid Decomposition on Pd−Au Bimetallic Surfaces. *J. Am. Chem. Soc.* **2014**, *136*, 11070−11078.
(131) Herron, J. A.; Scaranto, J.; Ferrin, P.; Li, S.; Mavrikakis, M. Trends in Formic Acid Decomposition on Model Transition Metal Surfaces: A Density Functional Theory Study. *ACS Catal.* **2014**, *4*, 4434−4445.
(132) Yoo, J. S.; Abild-Pedersen, F.; Nørskov, J. K.; Studt, F. Theoretical Analysis of Transition-Metal Catalysts for Formic Acid Decomposition. *ACS Catal.* **2014**, *4*, 1226−1233.
(133) Yuan, D.; Zhang, Y. Theoretical Investigations of HCOOH Decomposition on Ordered Cu-Pd Alloy Surfaces. *Appl. Surf. Sci.* **2018**, *462*, 649−658.
(134) Putra, S. E. M.; Muttaqien, F.; Hamamoto, Y.; Inagaki, K.; Hamada, I.; Morikawa, Y. Van Der Waals Density Functional Study of Formic Acid Adsorption and Decomposition on Cu(111). *J. Chem. Phys.* **2019**, *150*, 154707.
(135) Yuan, D. W.; Liu, Z. R. Atomic Ensemble Effects on Formic Acid Oxidation on PdAu Electrode Studied by First-Principles Calculations. *J. Power Sources* **2013**, *224*, 241−249.
(136) Yuan, D.; Gong, X.; Wu, R. Decomposition Pathways of Methanol on the PtAu(111) Bimetallic Surface: A First-Principles Study. *J. Chem. Phys.* **2008**, *128*, No. 064706.
(137) Persson, B. N. J.; Spencer, N. D. Sliding Friction: Physical Principles and Applications. *Physics Today* **1999**, *52*, 66−68.
(138) Persson, B. N. J. Theory of Friction and Boundary Lubrication. *Phys. Rev. B* **1993**, *48*, 18140−18158.
(139) Brigazzi, M.; Santoro, G.; Franchini, A.; Bortolani, V. Simulations of the Temperature Dependence of Static Friction at the $N_2$ /Pb Interface. *J. Phys.: Condens. Matter* **2007**, *19*, 305014.
(140) Franchini, A.; Brigazzi, M.; Santoro, G.; Bortolani, V. Theory of Static Friction: Temperature and Corrugation Effects. *J. Phys.: Condens. Matter* **2008**, *20*, 224019.
(141) Mo, Y.; Turner, K. T.; Szlufarska, I. Friction Laws at the Nanoscale. *Nature* **2009**, *457*, 1116−1119.
(142) Bortolani, V.; Franchini, A.; Santoro, G.; Brigazzi, M. Theory of Friction with Applied Load. *Tribol Lett* **2010**, *39*, 251−255.
(143) Persson, M. Possible Electronic Mechanism behind Nano-tribology of a Rare-Gas Monolayer. *Solid State Commun.* **1991**, *80*, 917−918.
(144) Hückstädt, C.; Schmidt, S.; Hüfner, S.; Forster, F.; Reinert, F.; Springborg, M. Work Function Studies of Rare-Gas/Noble Metal Adsorption Systems Using a Kelvin Probe. *Phys. Rev. B* **2006**, *73*, No. 075409.

(145) Lazić, P.; Crljen, Ž.; Brako, R.; Gumhalter, B. Role of van Der Waals Interactions in Adsorption of Xe on Cu(111) and Pt(111). *Phys. Rev. B* **2005**, *72*, 245407.
(146) Rohlfing, M.; Bredow, T. Binding Energy of Adsorbates on a Noble-Metal Surface: Exchange and Correlation Effects. *Phys. Rev. Lett.* **2008**, *101*, 266106.
(147) Román-Pérez, G.; Soler, J. M. Efficient Implementation of a van Der Waals Density Functional: Application to Double-Wall Carbon Nanotubes. *Phys. Rev. Lett.* **2009**, *103*, No. 096102.
(148) Zhang, W. B.; Chen, C.; Tang, P. Y. First-Principles Study for Stability and Binding Mechanism of Graphene/Ni(111) Interface: Role of VdW Interaction. *J. Chem. Phys.* **2014**, *141*, No. 044708.
(149) Zhang, Y. N.; Hanke, F.; Bortolani, V.; Persson, M.; Wu, R. Q. Why Sliding Friction of Ne and Kr Monolayers Is So Different on the Pb(111) Surface. *Phys. Rev. Lett.* **2011**, *106*, 236103.
(150) Ferralis, N.; Li, H. I.; Hanna, K. J.; Stevens, J.; Shin, H.; Pan, F. M.; Diehl, R. D. Structural and Thermal Properties of Xe on the Pb(111) Surface Studied by Low-Energy Electron Diffraction. *J. Phys.: Condens. Matter* **2007**, *19*, No. 056011.
(151) Voloshina, E. Local Correlation Method for Metals: Benchmarks for Surface and Adsorption Energies. *Phys. Rev. B* **2012**, *85*, No. 045444.
(152) Dion, M.; Rydberg, H.; Schröder, E.; Langreth, D. C.; Lundqvist, B. I. Erratum: Van Der Waals Density Functional for General Geometries [Phys. Rev. Lett. **92**, 246401 (2004)]. *Phys. Rev. Lett.* **2005**, *95*, 109902.
(153) Langreth, D. C.; Lundqvist, B. I.; Chakarova-Käck, S. D.; Cooper, V. R.; Dion, M.; Hyldgaard, P.; Kelkkanen, A.; Kleis, J.; Kong, L.; Li, S.; Moses, P. G.; Murray, E.; Puzder, A.; Rydberg, H.; Schröder, E.; Thonhauser, T. A Density Functional for Sparse Matter. *J. Phys.: Condens. Matter* **2009**, *21*, No. 084203.
(154) Chen, D.-L.; Al-Saidi, W. A.; Johnson, J. K. Noble Gases on Metal Surfaces: Insights on Adsorption Site Preference. *Phys. Rev. B* **2011**, *84*, 241405.
(155) Zhang, Y. N.; Bortolani, V.; Mistura, G. Determination of Corrugation and Friction of Cu(111) toward Adsorption and Motion of Ne and Xe. *Phys. Rev. B* **2014**, *89*, 165414.
(156) Krim, J.; Widom, A. Damping of a Crystal Oscillator by an Adsorbed Monolayer and Its Relation to Interfacial Viscosity. *Phys. Rev. B* **1988**, *38*, 12184−12189.
(157) Annett, J. F.; Haydock, R. Anticorrugating Effect of Hybridization on the Helium Diffraction Potential for Metal Surfaces. *Phys. Rev. Lett.* **1984**, *53*, 838−841.
(158) Ambrosetti, A.; Silvestrelli, P. L. Van Der Waals Interactions in Density Functional Theory Using Wannier Functions: Improved $C_6$ and $C_3$ Coefficients by a Different Approach. *Phys. Rev. B* **2012**, *85*, No. 073101.
(159) Silvestrelli, P. L.; Ambrosetti, A. Inclusion of Screening Effects in the van Der Waals Corrected DFT Simulation of Adsorption Processes on Metal Surfaces. *Phys. Rev. B* **2013**, *87*, No. 075401.
(160) Silvestrelli, P. L.; Ambrosetti, A. Van Der Waals Corrected DFT Simulation of Adsorption Processes on Transition-Metal Surfaces: Xe and Graphene on Ni(111). *Phys. Rev. B* **2015**, *91*, 195405.
(161) Silvestrelli, P. L.; Ambrosetti, A. Van Der Waals-Corrected Density Functional Theory Simulation of Adsorption Processes on Noble-Metal Surfaces: Xe on Ag(111), Au(111), and Cu(111). *J. Low Temp. Phys.* **2016**, *185*, 183−197.
(162) Ruiz, V. G.; Liu, W.; Tkatchenko, A. Density-Functional Theory with Screened van Der Waals Interactions Applied to Atomic and Molecular Adsorbates on Close-Packed and Non-Close-Packed Surfaces. *Phys. Rev. B* **2016**, *93*, No. 035118.
(163) Terentjev, A. V.; Constantin, L. A.; Pitarke, J. M. Dispersion-Corrected PBEsol Exchange-Correlation Functional. *Phys. Rev. B* **2018**, *98*, 214108.
(164) Terentjev, A. V.; Constantin, L. A.; Artacho, E.; Pitarke, J. M. Comparison of Dispersion-Corrected Exchange-Correlation Functionals Using Atomic Orbitals. *Phys. Rev. B* **2019**, *100*, 235439.
(165) Benedek, G. *Helium Atom Scattering from Surfaces*; Hulpke, E., Ertl, G., Gomer, R., Mills, D. L., Lotsch, H. K. V., Eds.;Springer Series in Surface Sciences; Springer Berlin Heidelberg: Berlin, Heidelberg, 1992; Vol. *27*.
(166) Rieder, K. H.; Parschau, G.; Burg, B. Experimental Evidence for Anticorrugating Effects in He-Metal Interactions at Surfaces. *Phys. Rev. Lett.* **1993**, *71*, 1059−1062.
(167) Petersen, M.; Wilke, S.; Ruggerone, P.; Kohler, B.; Scheffler, M. Scattering of Rare-Gas Atoms at a Metal Surface: Evidence of Anticorrugation of the Helium-Atom Potential Energy Surface and the Surface Electron Density. *Phys. Rev. Lett.* **1996**, *76*, 995−998.
(168) Esbjerg, N.; Nørskov, J. K. Dependence of the He-Scattering Potential at Surfaces on the Surface-Electron-Density Profile. *Phys. Rev. Lett.* **1980**, *45*, 807−810.
(169) Sun, J.; Zhang, Y.; Lu, Z.; Xue, Q.; Wang, L. Attraction Induced Frictionless Sliding of Rare Gas Monolayer on Metallic Surfaces: An Efficient Strategy for Superlubricity. *Phys. Chem. Chem. Phys.* **2017**, *19*, 11026−11031.
(170) Sun, J.; Zhang, Y.; Lu, Z.; Li, Q.; Xue, Q.; Du, S.; Pu, J.; Wang, L. Superlubricity Enabled by Pressure-Induced Friction Collapse. *J. Phys. Chem. Lett.* **2018**, *9*, 2554−2559.
(171) Dobson, J. F. Beyond Pairwise Additivity in London Dispersion Interactions. *Int. J. Quantum Chem.* **2014**, *114*, 1157−1161.
(172) Feynman, R. P. Forces in Molecules. *Phys. Rev.* **1939**, *56*, 340−343.


https://dx.doi.org/10.1021/acs.jpcc.0c02293
J. Phys. Chem. C 2020, 124, 16926−16942